Retinal output

Retinal input

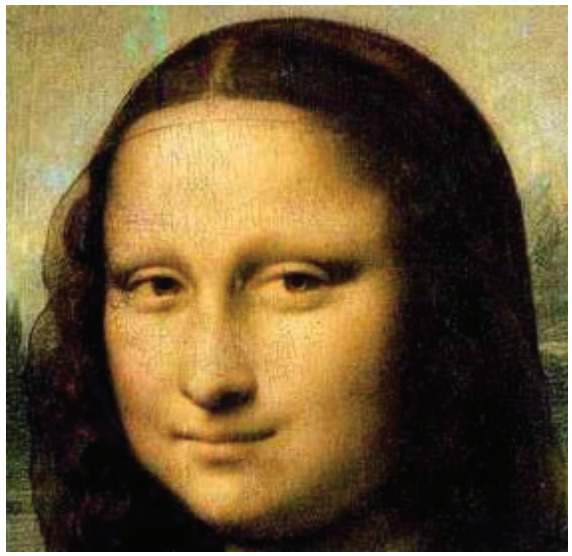

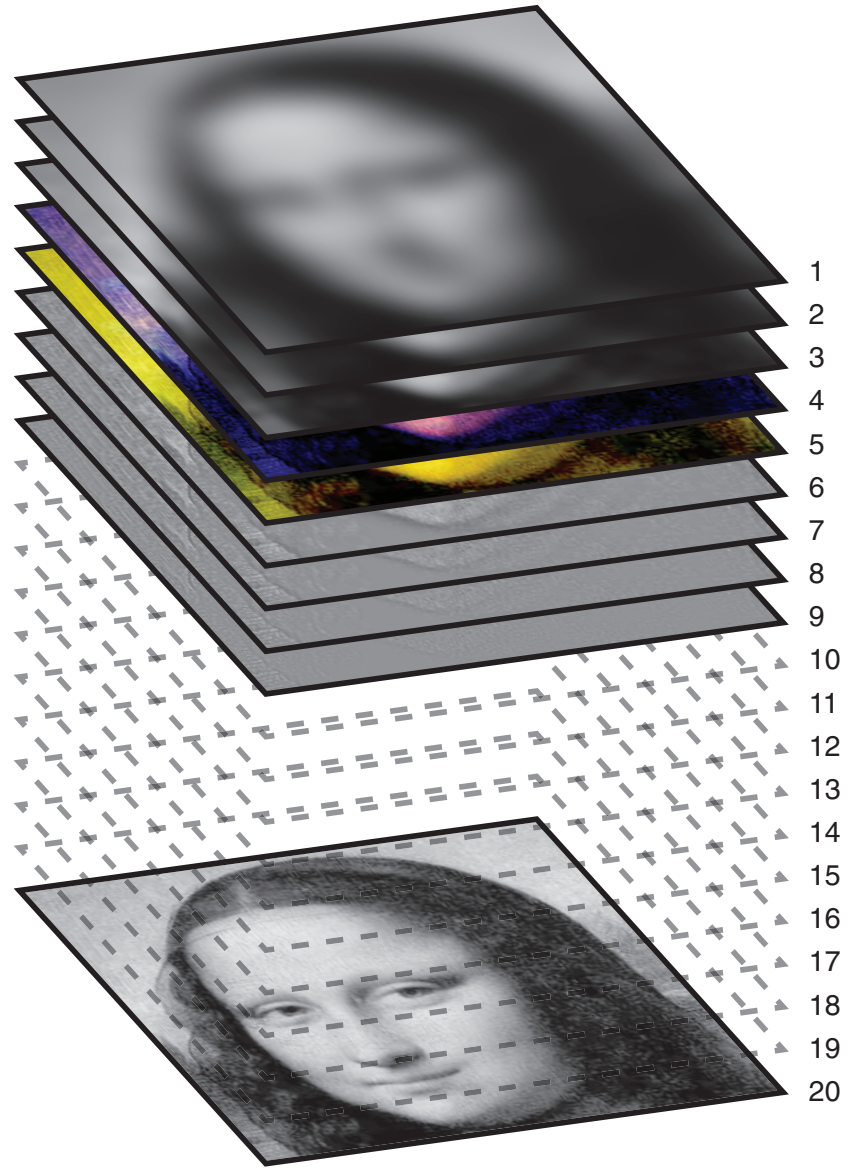

The retina creates 20 neural representations of the “movie” that enters the eye.

Roska and Meister, 2014

Morphology, mosaics and targets of diverse ganglion cell populations in macaque retina: approaching a complete account

D.M. Dacey, H.R. Joo, B.B. Peterson, T.J. Haun
Department of Biological Structure, University of Washington, Seattle WA

Purpose

Our goal is a complete description of primate visual pathway origins, providing an anatomical basis for targeted physiological analysis, dissection of underlying circuitry and for making trans-species comparisons, most notably with the mouse, for which transgenic technology offers increasing access to retinal pathways.

Methods

To observe the morphology of macaque ganglion cells we used the 'fireworks' photostaining technique (Dacey et al., Neuron 2003, 37:15) from central tracer injections made into the lateral geniculate nucleus (LGN) or the superior colliculus-pretectum. Fireworks staining completely reveals the dendritic trees of large numbers of retrogradely labeled ganglion cells. In this way we can measure type-specific stratification depth in the inner plexiform layer and relative density from the mosaics formed by overlapping dendritic trees of the same type. (Right: photostained cells retrogradely tracer labeled from injections in the superior colliculus.)

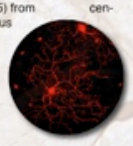

Smooth monostratified

inner ON-center and outer OFF-center types
transient, achromatic, Y-cell receptive field*

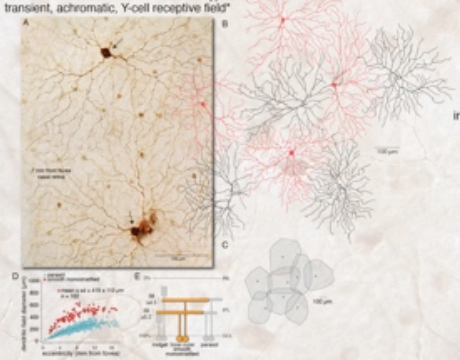

Smooth monostratified cells comprise ~2.5% of total ganglion cells (coverage: inner cells 1.4; outer cells 1.4) and project to the LGN, superior colliculus and pretectum. **A**. Photomicrograph of two smooth cells intracellularly injected with Neurobiotin and processed for HRP histochemistry. The smooth cells are tracer coupled to a population of small bodied amacrine cells. **B**. Tracings of 8 inner smooth cells ~7 mm from the fovea, tracer labeled from injections in the superior colliculus and processed for HRP histochemistry. **C**. Outlines of the overlapping dendritic fields of the 8 cells shown in *B*. **D**. Dendritic field diameter plotted as a function of eccentricity. **E**. Mean dendritic stratification measured relative to parasol stratification in wholemount retina and plotted as percentage depth in the IPL (inner smooth/parasol cell pairs, n = 4; outer smooth/parasol cell pairs, n = 20). (GCL: ganglion cell layer; IPL: inner plexiform layer; INL: inner nuclear layer.)

*Crook et al., J Neurosci 2008, 28(48):12654

Parasol

inner ON-center and outer OFF-center types
primate correlate of the alpha Y-cell*

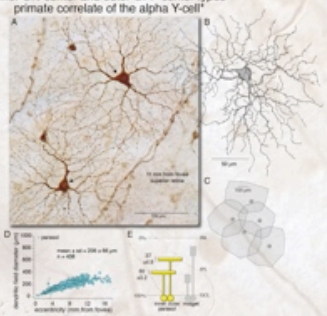

Parasol cells comprise ~14% of total ganglion cells (coverage: inner cells 1.9; outer cells 1.6) and project to the LGN, superior colliculus and pretectum. **A**. Photomicrograph of two photostained cells tracer labeled from injections in the superior colliculus and reacted for HRP histochemistry. **B**. Tracing of an inner parasol cell 8.7 mm from the fovea (dendritic field diameter = 213 µm). Arrow indicates axon. **C**. Outlines of the overlapping dendritic fields of 5 neighboring outer parasol cells ~6 mm from the fovea. **D**. Dendritic field diameter plotted as a function of eccentricity. **E**. Mean dendritic stratification measured in wholemount retina and plotted as percentage depth in the IPL (inner cells, n = 36; outer cells, n = 20).

*Crook et al., J Neurosci 2008, 28(44):11277

Midget

inner ON-center and outer OFF-center types

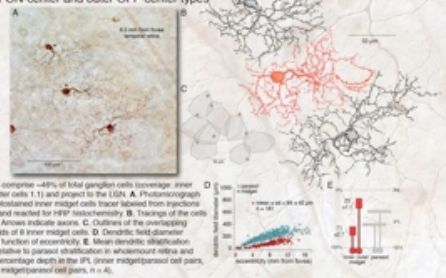

Midget cells comprise ~46% of total ganglion cells (coverage: inner cells 1.1; outer cells 1.1) and project to the LGN. **A**. Photomicrograph of three photostained inner midget cells tracer labeled from injections in the LGN and reacted for HRP histochemistry. **B**. Tracings of the cells shown in *A*. Arrows indicate axons. **C**. Outlines of the overlapping dendritic fields of 8 inner midget cells. **D**. Dendritic field diameter plotted as a function of eccentricity. **E**. Mean dendritic stratification measured relative to parasol stratification in wholemount retina and plotted as percentage depth in the IPL (inner midget/parasol cell pairs, n = 4; outer midget/parasol cell pairs, n = 4).

Small bistratified

'blue-ON' cell; S vs LM cone opponency

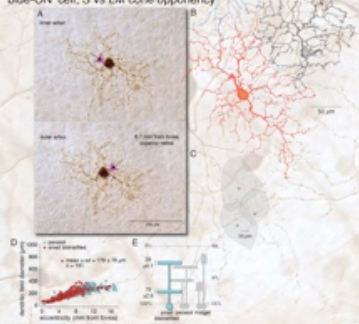

Small bistratified cells make up ~8% of total ganglion cells (coverage = 1.6) and project to the LGN. **A**. Photomicrographs of a small bistratified cell intracellularly injected with Neurobiotin and processed for HRP histochemistry, with the focus on the inner (upper) and outer (lower) dendritic arbors. **B**. Tracings of the inner arbors of 3 neighboring small bistratified cells ~9-8 mm from the fovea, tracer labeled from injections in the LGN and processed for HRP histochemistry. Overlapping dendrites show cofasciculation. Arrows indicate axons. **C**. Outlines of the overlapping dendritic fields of the 3 cells shown in *B*. **D**. Dendritic field diameter plotted as a function of eccentricity. **E**. Mean dendritic stratification measured relative to parasol stratification in wholemount retina and plotted as percentage depth in the IPL (parasol/small bistratified pairs: n = 11).

Large bistratified

second type of S-opponent 'blue-ON' cell

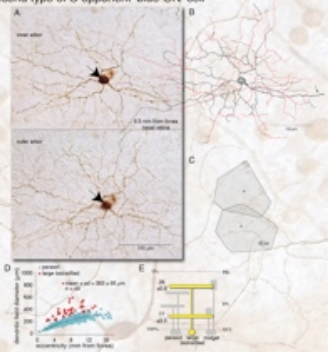

Large bistratified cells make up ~3% of total ganglion cells (coverage: ~ 2) and project to the LGN. **A**. Photomicrographs of a large bistratified cell intracellularly injected with Neurobiotin and processed for HRP histochemistry. Focus is on the inner (upper) and outer (lower) dendritic arbors. **B**. Tracing of the same cell shown in *A*. Outer dendritic arbor is shown in red. Arrow indicates axon. **C**. Outlines of the dendritic fields of two neighboring large bistratified cells with overlapping dendritic fields. **D**. Dendritic field diameter plotted as a function of eccentricity. **E**. Mean dendritic stratification measured relative to parasol stratification in wholemount retina and plotted as percentage depth in the IPL (parasol/large bistratified cell pairs: n = 5).

Recursive bistratified

primate candidate for the ON-OFF direction selective type

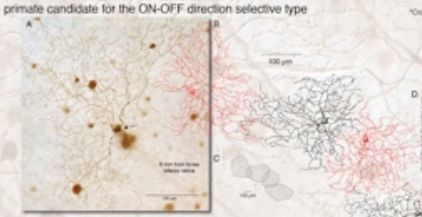

Recursive bistratified cells comprise ~1.5% of total ganglion cells (coverage = 1.3) and project to the LGN, superior colliculus and pretectum. **A**. Photomicrograph of a recursive bistratified cell intracellularly injected with Neurobiotin and processed for HRP histochemistry. The cell shows tracer coupling to large and small bodied amacrine cell populations. **B**. Tracings of 7 cells ~7 mm from the fovea, tracer labeled from injections in the superior colliculus and processed for HRP histochemistry. **C**. Outlines of the overlapping dendritic fields of the 7 cells shown in *B*. **D**. Dendritic field diameter plotted as a function of eccentricity. **E**. Mean dendritic stratification measured relative to parasol stratification in wholemount retina and plotted as percentage depth in the IPL (recursive bistratified/parasol cell pairs, n = 3).

Narrow thorny

inner and outer types, transient, achromatic

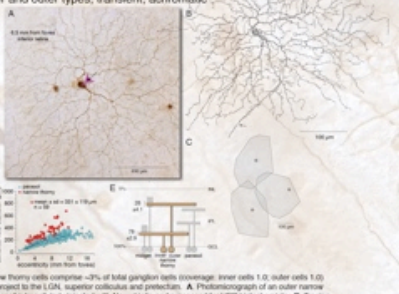

Narrow thorny cells comprise ~3% of total ganglion cells (coverage: inner cells 1.0; outer cells 1.0) and project to the LGN, superior colliculus and pretectum. **A**. Photomicrograph of an outer narrow thorny cell intracellularly injected with Neurobiotin and processed for HRP histochemistry. **B**. Tracing of the same cell shown in *A*. Arrow indicates axon. **C**. Outlines of the overlapping dendritic fields of 3 neighboring outer narrow thorny cells tracer labeled from injections in the superior colliculus. **D**. Dendritic field diameter plotted as a function of eccentricity. **E**. Mean dendritic stratification measured relative to parasol stratification in wholemount retina and plotted as percentage depth in the IPL (inner narrow thorny/parasol cell pairs, n = 4; outer narrow thorny/parasol cell pairs, n = 4).

Recursive monostratified

primate candidate for the ON direction selective type

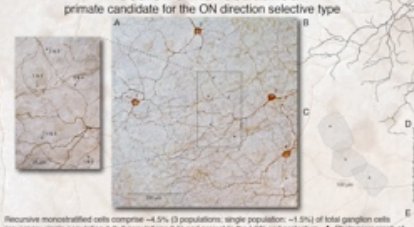

Recursive monostratified cells comprise ~4.5% (3 populations: single population: ~1.5%) of total ganglion cells (coverage: single population 1.2; 3 populations 3.5) and project to the LGN and pretectum. **A**. Photomicrograph of photostained cells tracer labeled from injections in the pretectum and reacted for HRP histochemistry. Dendrites of the four labeled cells and other nearby cells (cell bodies not shown) form a dense plexis of cofasciculated processes. Inset: Magnified view of boxed area in *A*. Arrows indicate 5 examples of cofasciculation. Numbers correspond to the dendrites' cells of origin as shown in *A*. **B**. Tracing of a recursive monostratified cell 8.9 mm from the fovea (dendritic field diameter = 399 µm). Arrow indicates axon. **C**. Outlines of the overlapping dendritic fields of 3 neighboring recursive monostratified cells ~8.8 mm from the fovea. **D**. Dendritic field diameter plotted as a function of eccentricity. **E**. Mean dendritic stratification measured relative to parasol stratification in wholemount retina and plotted as percentage depth in the IPL (recursive monostratified/inner parasol cell pairs, n = 3).

Melanopsin-expressing

inner and outer types, inherently photosensitive; S-OFF opponency

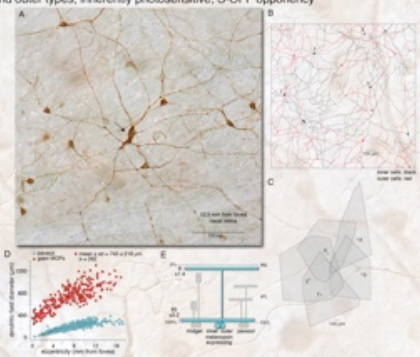

Giant melanopsin cells comprise ~1% of total ganglion cells (coverage: inner cells 1.5; outer cells 2.0) and project to the LGN, superior colliculus and pretectum. **A**. Photomicrograph of a giant melanopsin cell intracellularly injected with Neurobiotin and processed for HRP histochemistry. The cell shows tracer coupling to several populations of amacrine cells. **B**. Tracings of 7 inner (black) and 8 outer (red) giant cells ~10 mm from the fovea, melanopsin immunolabeled and processed for HRP histochemistry. **C**. Outlines of the overlapping dendritic fields of 5 inner giant cells. Numbers correspond to cells shown in *B*. **D**. Dendritic field diameter plotted as a function of eccentricity. **E**. Mean dendritic stratification measured relative to parasol stratification in wholemount retina and plotted as percentage depth in the IPL (inner giant melanopsin/parasol cell pairs, n = 3; outer giant melanopsin/parasol cell pairs, n = 5).

Broad thorny

ON-OFF receptive field
primate candidate for the local edge detector

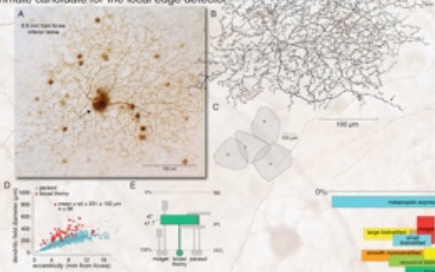

Broad thorny cells make up ~1.5% of total ganglion cells (coverage = 1.2) and project to the LGN, superior colliculus and pretectum. **A**. Photomicrograph of a broad thorny cell intracellularly injected with Neurobiotin and processed for HRP histochemistry. **B**. Tracing of the same cell shown in *A*. Arrow indicates axon. **C**. Outlines of the overlapping dendritic fields of 4 neighboring broad thorny cells ~5 mm from the fovea, tracer labeled from injections in the superior colliculus. **D**. Dendritic field diameter plotted as a function of eccentricity. **E**. Mean dendritic stratification measured relative to parasol stratification in wholemount retina and plotted as percentage depth in the IPL (broad thorny/parasol cell pairs: n = 8).

Schematic summary of dendritic stratification. Lengths of colored bars are proportional to dendritic field diameter for each cell type relative to parasol cell diameter. Vertical positioning of each bar is centered on the mean stratification depth for that cell type (values not shown). Widths of the bars are arbitrary for all cell types except midget and broad thorny cells, where it represents the mean innermost and outermost dendrites for these broadly stratifying cell types.

Conclusions

- The 17 cell populations shown here represent ~ 85% of the total number of ganglion cells.*
- At least 3 other cell types have been identified:
  - axon collateral-bearing ganglion cells (Peterson & Dacey, Vis Neurosci 1998, 15:377)
  - large, sparsely branched monostratified cells (inner and outer types).
- Taken together, and assuming ~ 2% density for the remaining 3 cell types, the 20 types account for ~ 90% of the ganglion cells. If multiple ON-OFF direction selective mosaics exist in primate (as found in other mammals) another ~5% would be accounted for.

*Total ganglion cell density is from Wässle et al., Nature 1989, 341:643. Density estimates for individual cell types were derived from the mosaics.

Midget

inner ON-center and outer OFF-center types

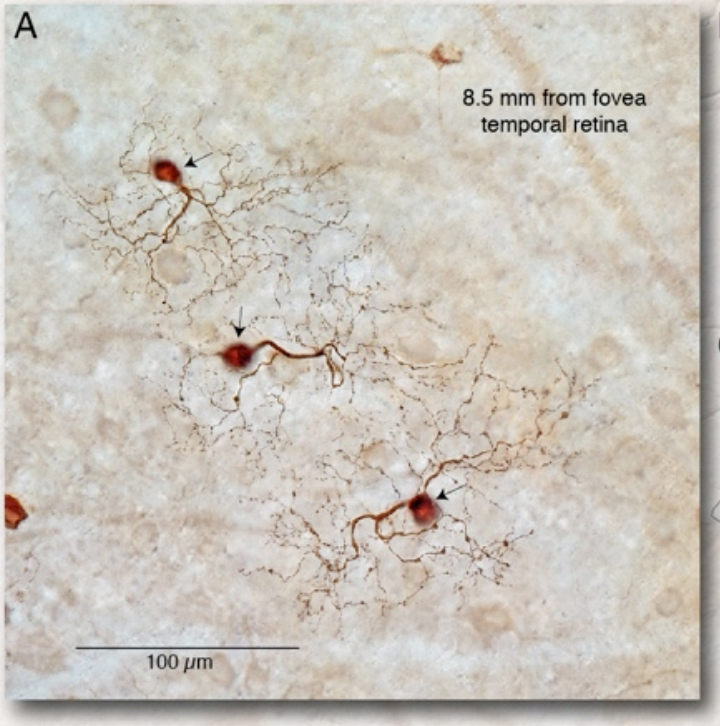

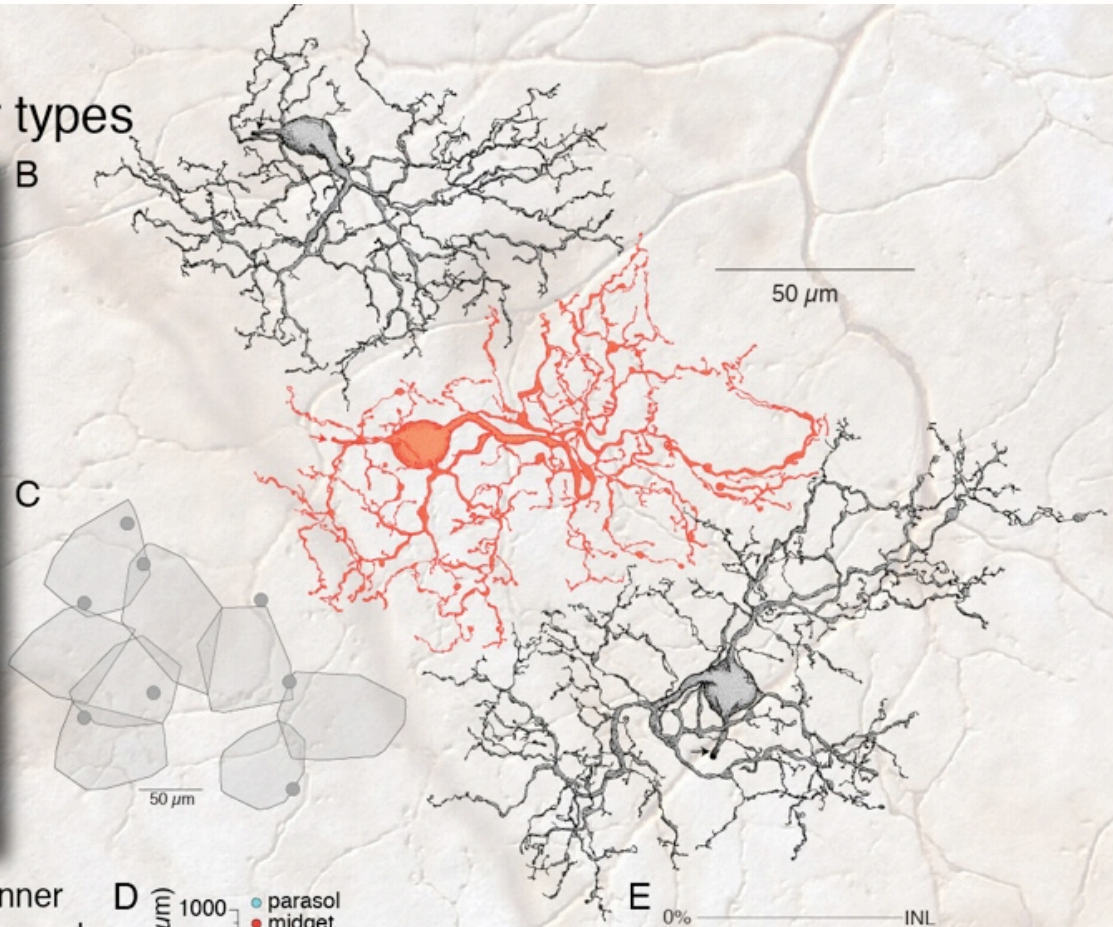

Midget cells comprise ~46% of total ganglion cells (coverage: inner cells 1.1; outer cells 1.1) and project to the LGN. **A**. Photomicrograph of three photostained inner midget cells tracer labeled from injections in the LGN and reacted for HRP histochemistry. **B**. Tracings of the cells shown in *A*. Arrows indicate axons. **C**. Outlines of the overlapping dendritic fields of 8 inner midget cells. **D**. Dendritic field diameter plotted as a function of eccentricity. **E**. Mean dendritic stratification measured relative to parasol stratification in wholemount retina and plotted as percentage depth in the IPL (inner midget/parasol cell pairs, n = 4; outer midget/parasol cell pairs, n = 4).

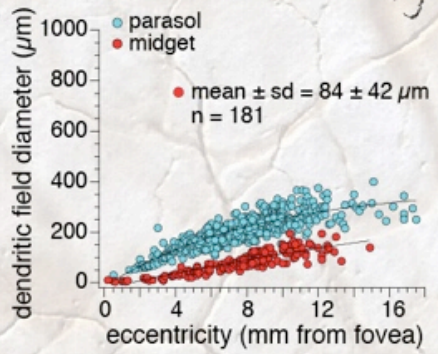

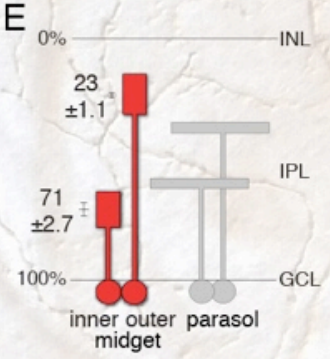

Diversity of ganglion cell morphology in mammalian retina

Icon	Mouse	Rabbit	Cat	Macaque	Properties
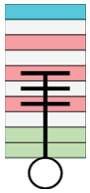				ON midget[22]	Small dendritic field. ON response.
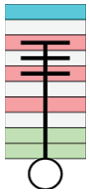				OFF midget[22]	Small dendritic field. OFF response.

Roska and Meister, 2014

Spatio-chromatic types of macaque LGN cells

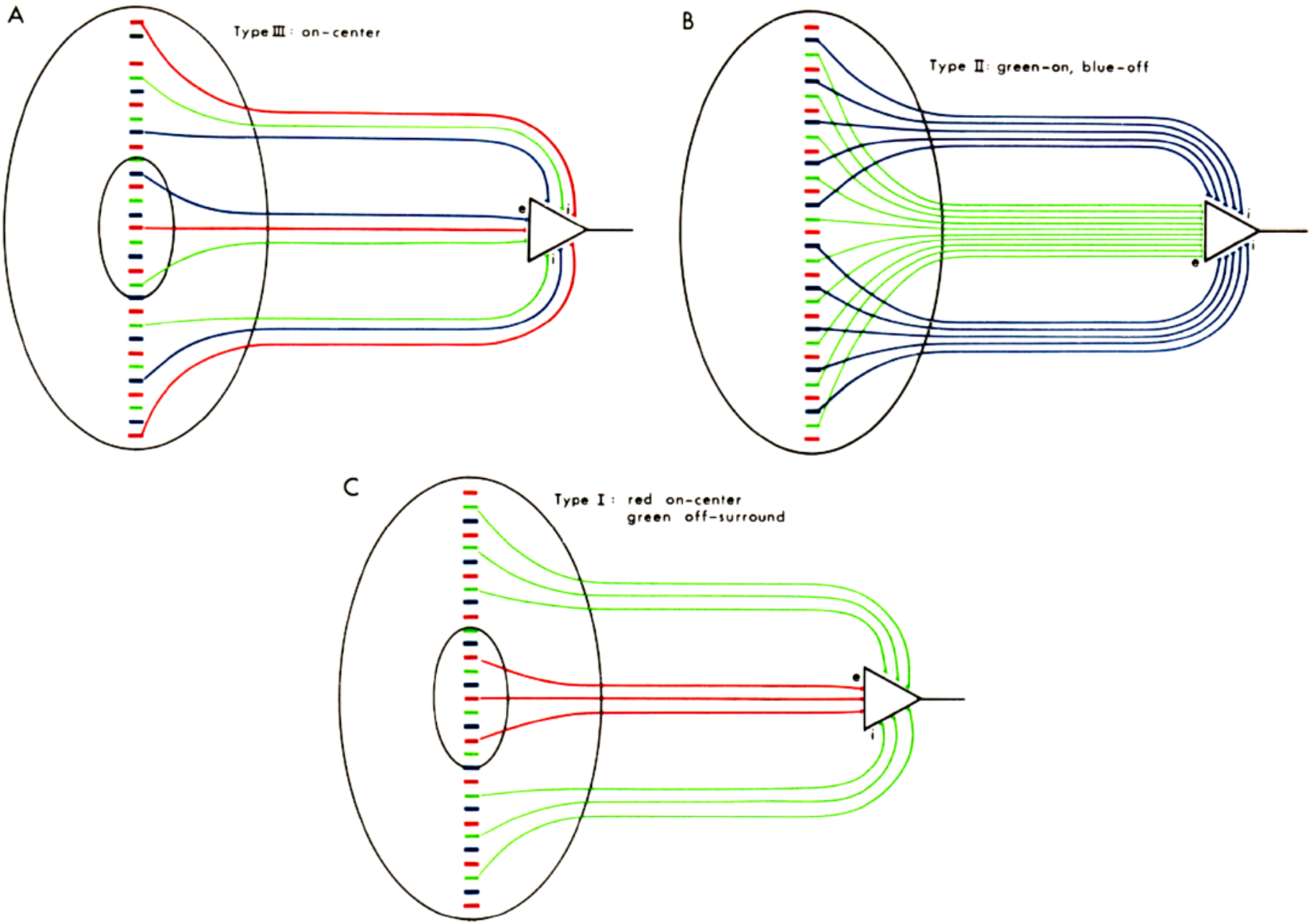

Wiesel & Hubel, 1966

Color-opponent midget cells: a primate specialization

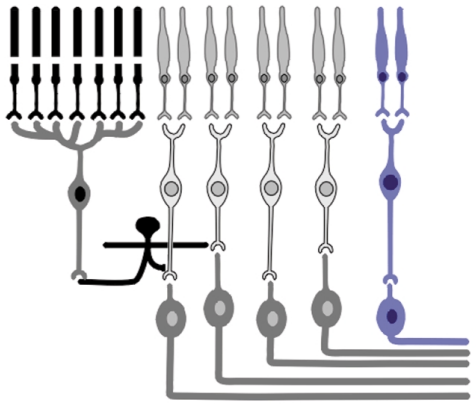

Primates →

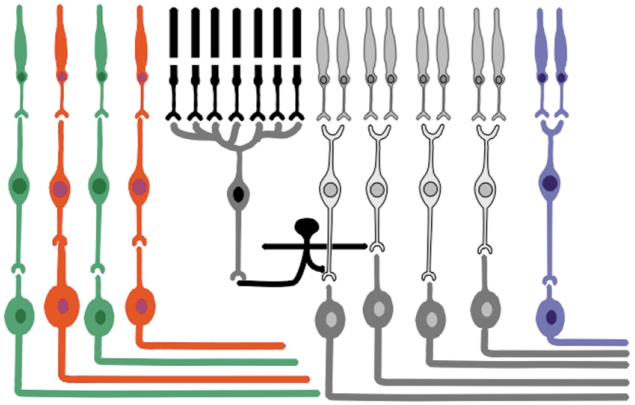

Generic mammalian retina

Primate Color Opponent Ganglion Cells

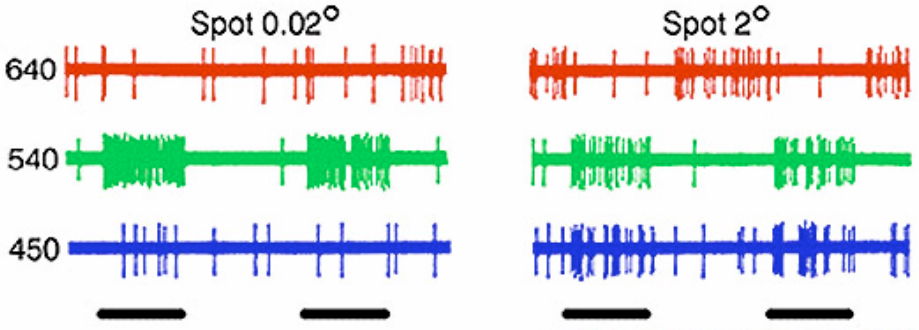

DeMonasterio & Gouras (1975)

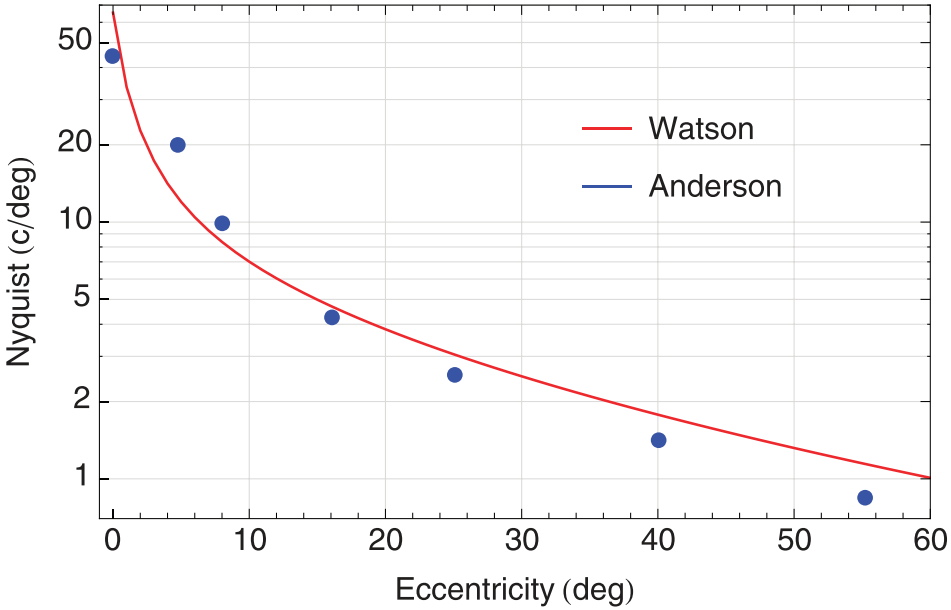

Inferred Receptive Field Description

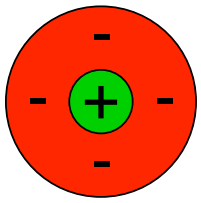

Masland, 2001;
DeMonasterios & Gouras, 1975;
Watson, 2014

Midget ganglion cells show red-green L vs M cone opponency

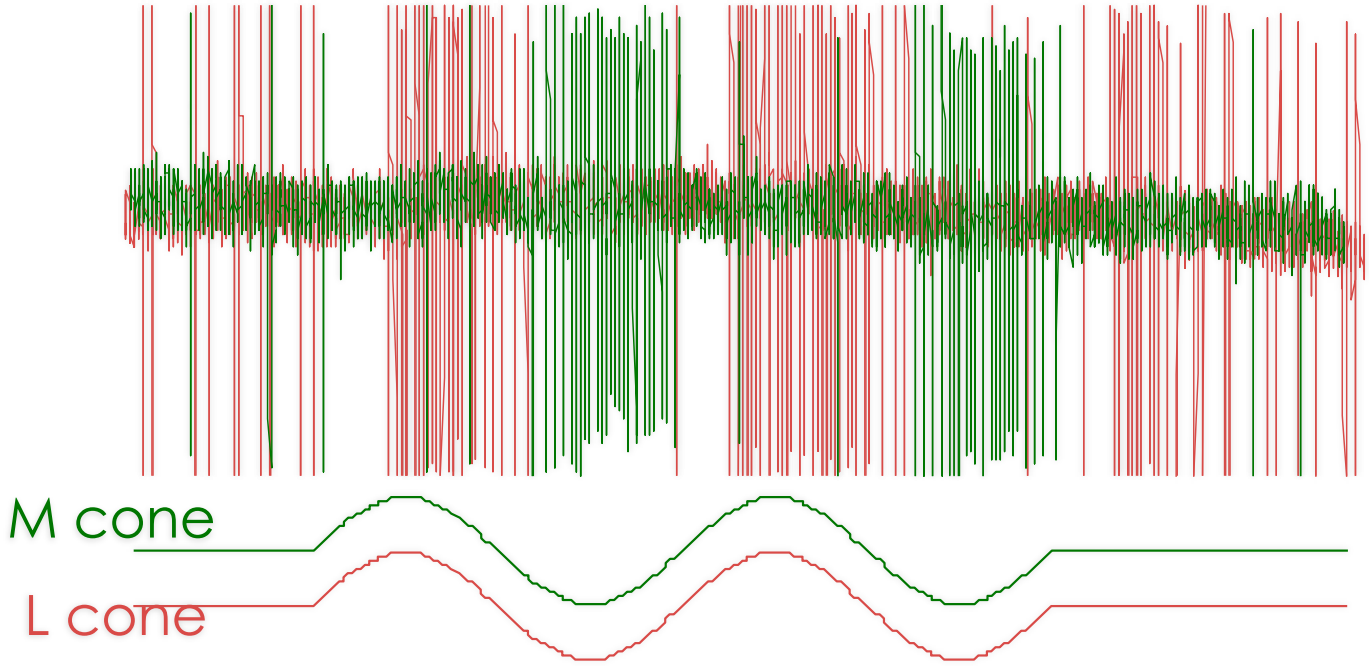

Jo Crook & Dennis Dacey

Random-wiring
achromatic-chromatic

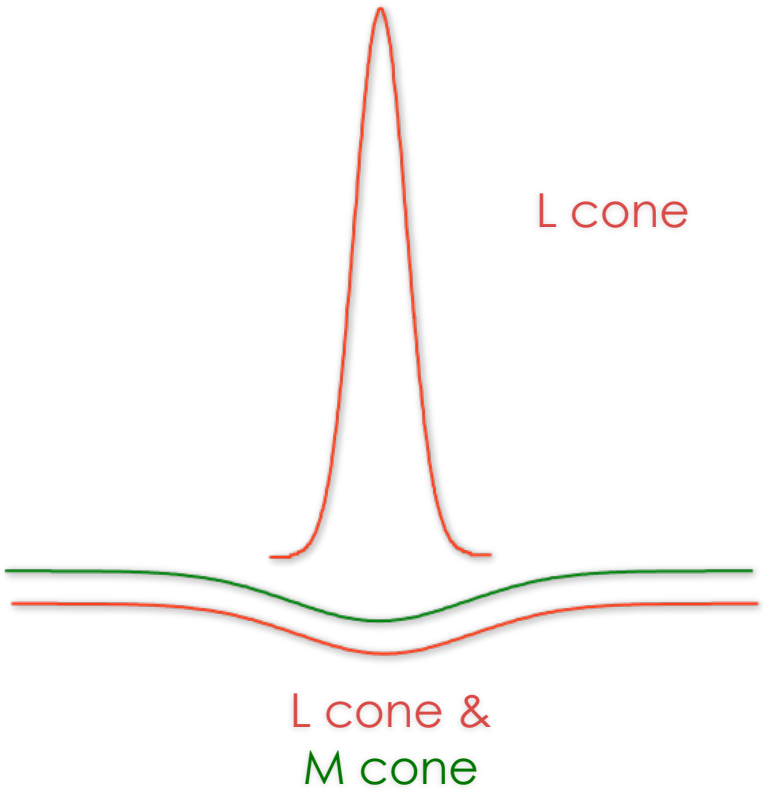

e.g. Paulus & Kroger-Paulus, 1983
Lennie et al., 1991

Cone-selective
pure color

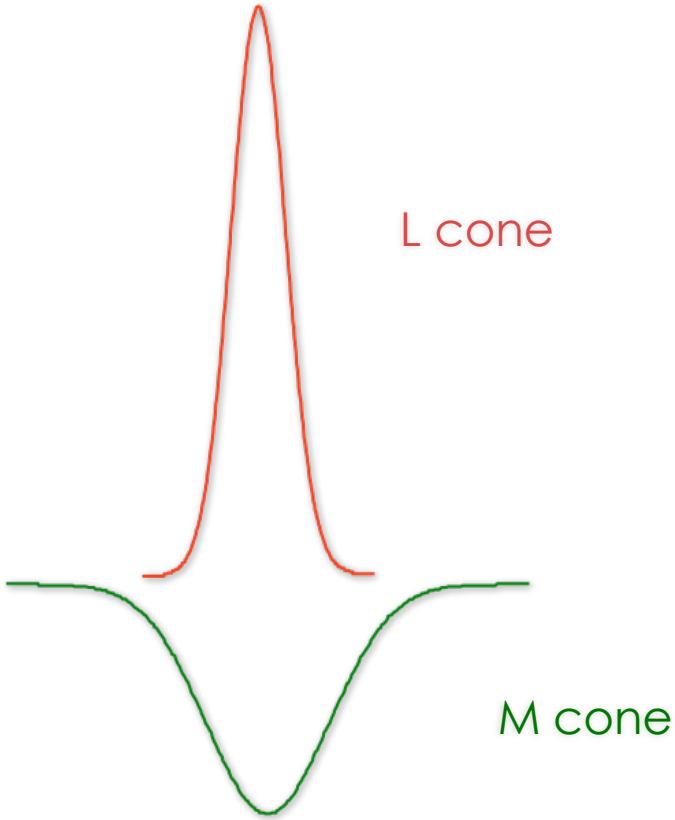

Shapley & Perry, 1986
Lee, 1999
Reid & Shapley, 2002
Shapley, 2006
Buzas et al., 2006

Jo Crook & Dennis Dacey

Data from midget cells with multiple cone inputs to the receptive field center

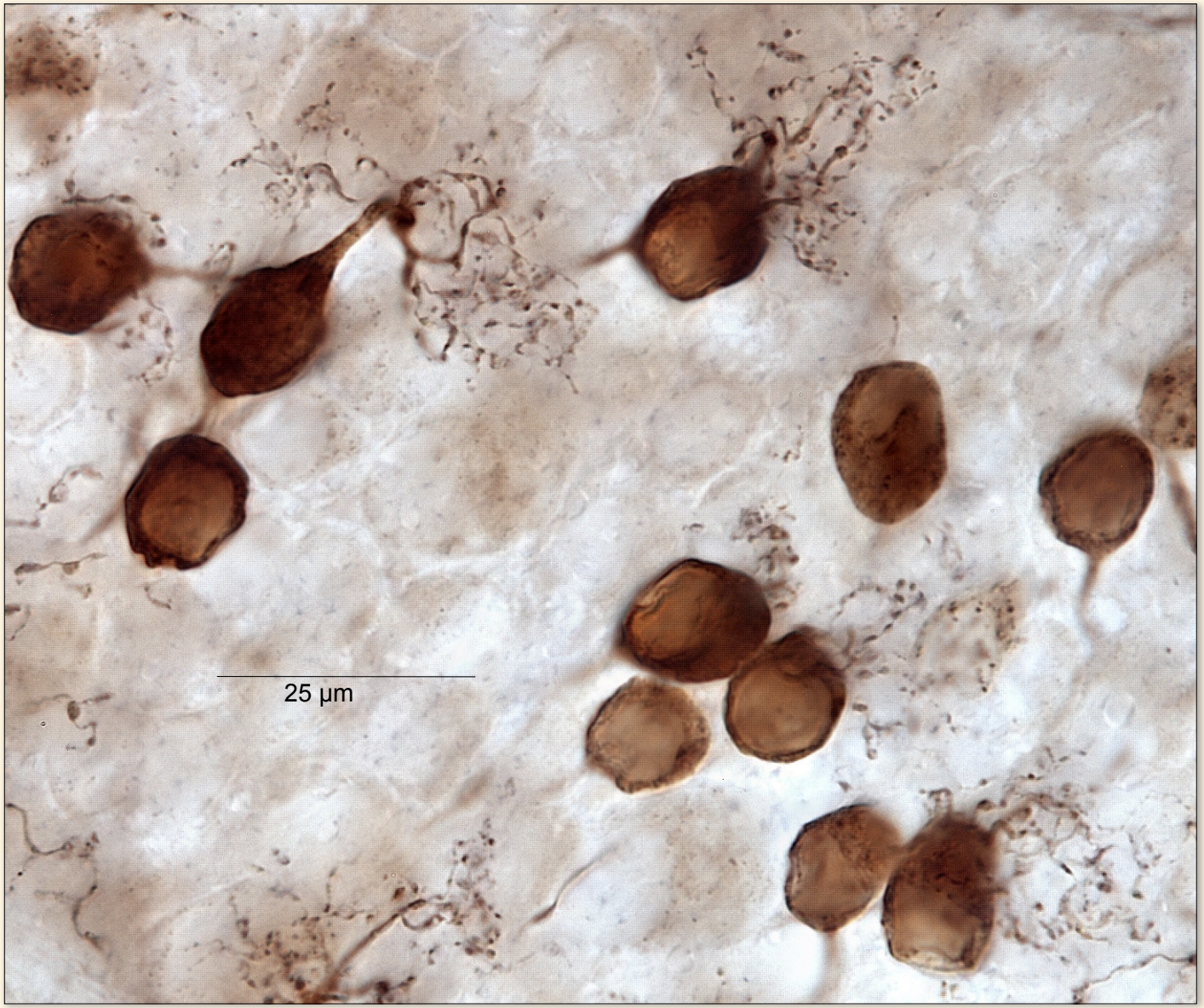

Jo Crook & Dennis Dacey

Record from midget cells with multiple cone inputs to the receptive field center

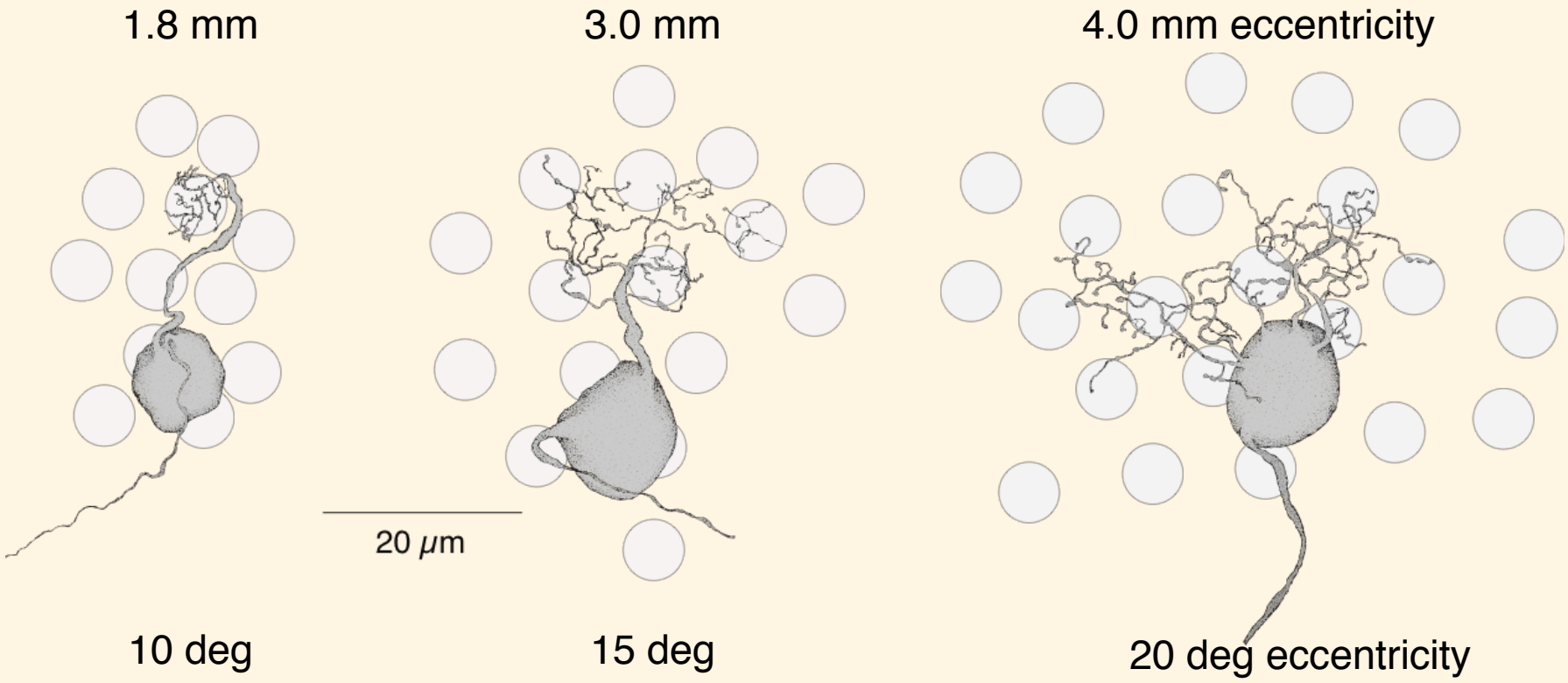

Martin et al., 2001
Solomon et al., 2005
Buzas et al., 2006

Jo Crook & Dennis Dacey

Mosaic of Red, Green and Blue Cones of the Living Human Retina

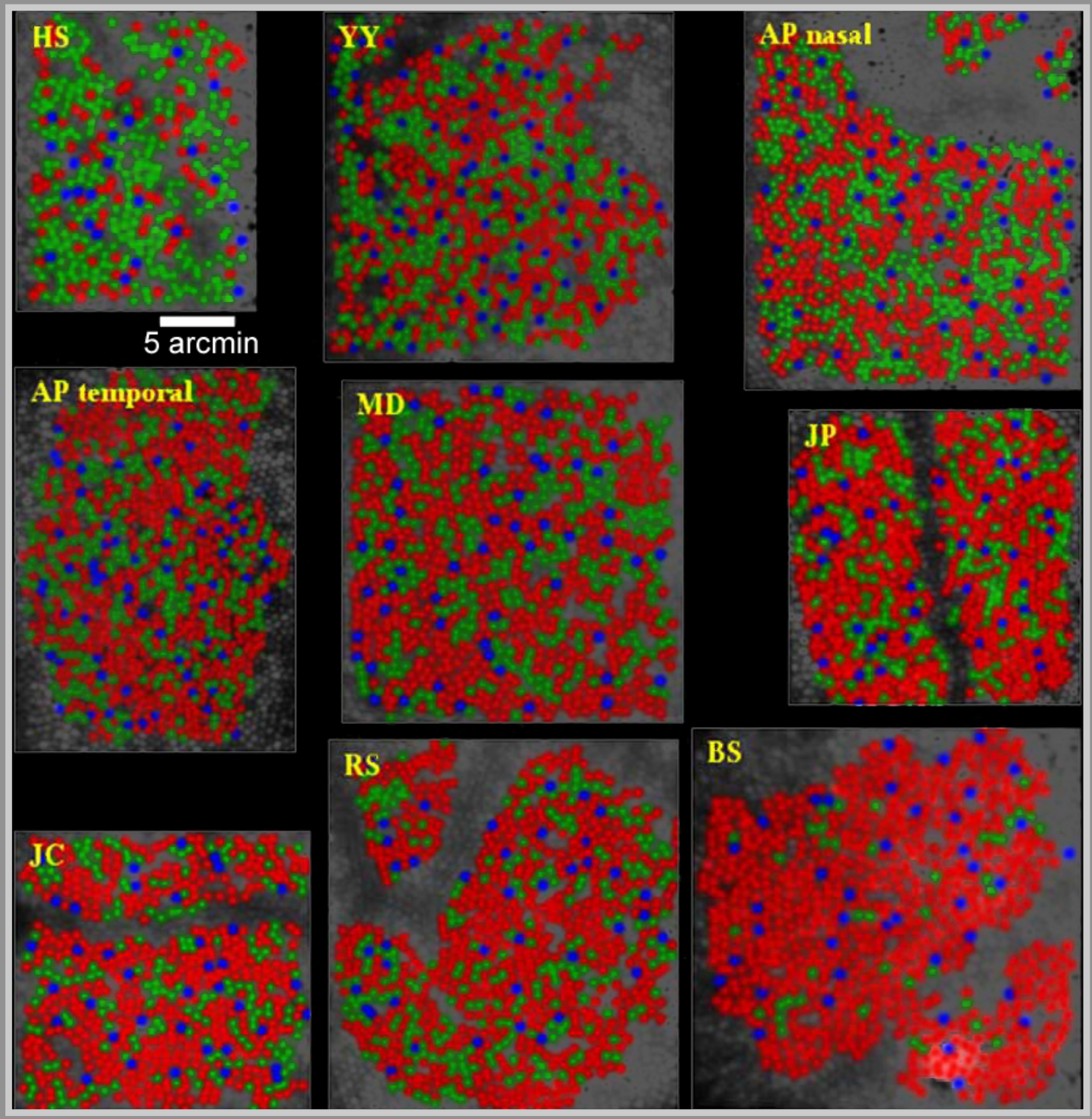

Hofer et al. (2005)

Cone inputs to the receptive field suggest random wiring

Chromatic midgets
(n = 109)

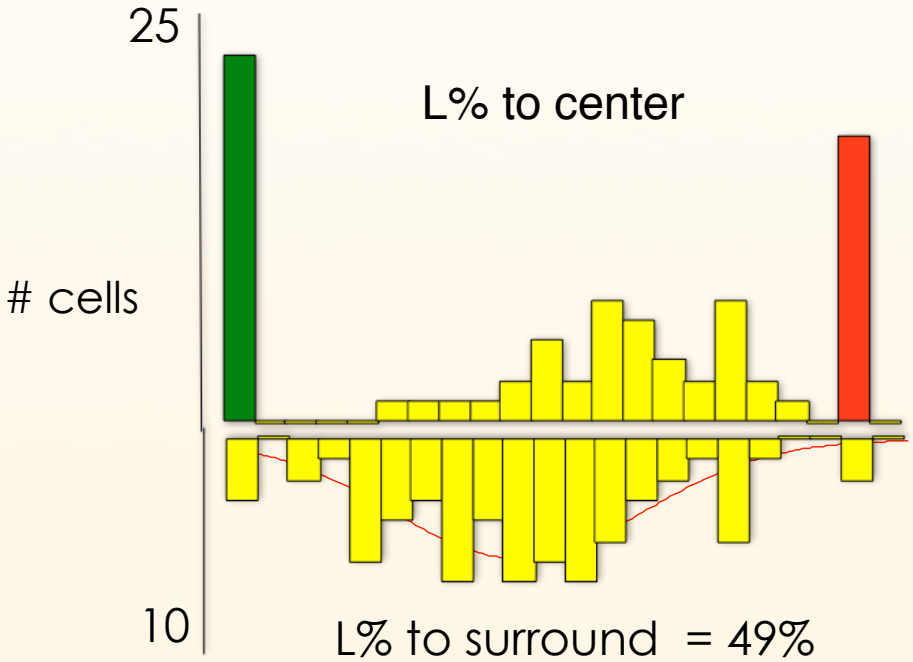

Achromatic midgets
(n = 74)

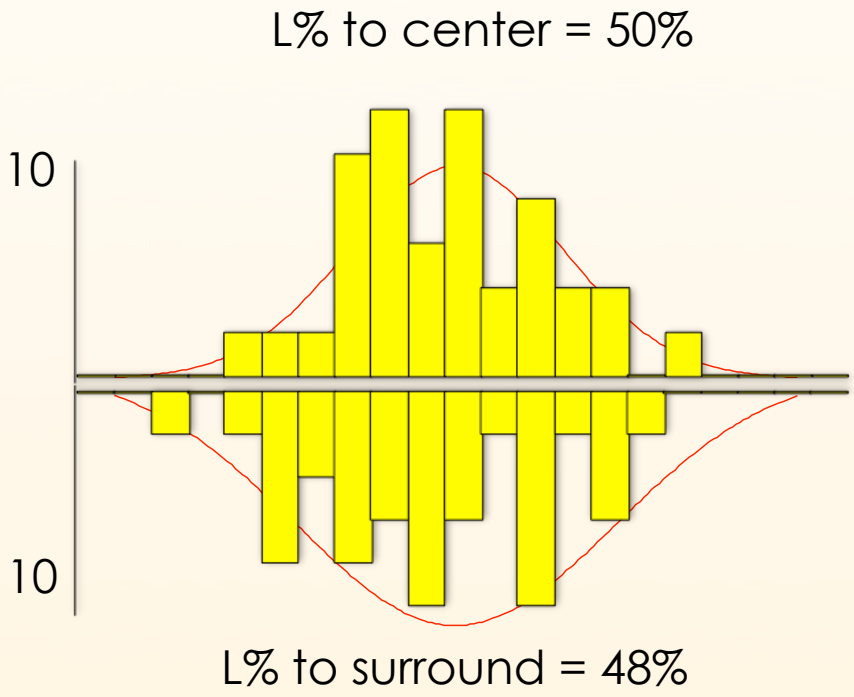

L% input L/(L+M)

Jo Crook & Dennis Dacey

Cone inputs to the receptive field suggest random wiring

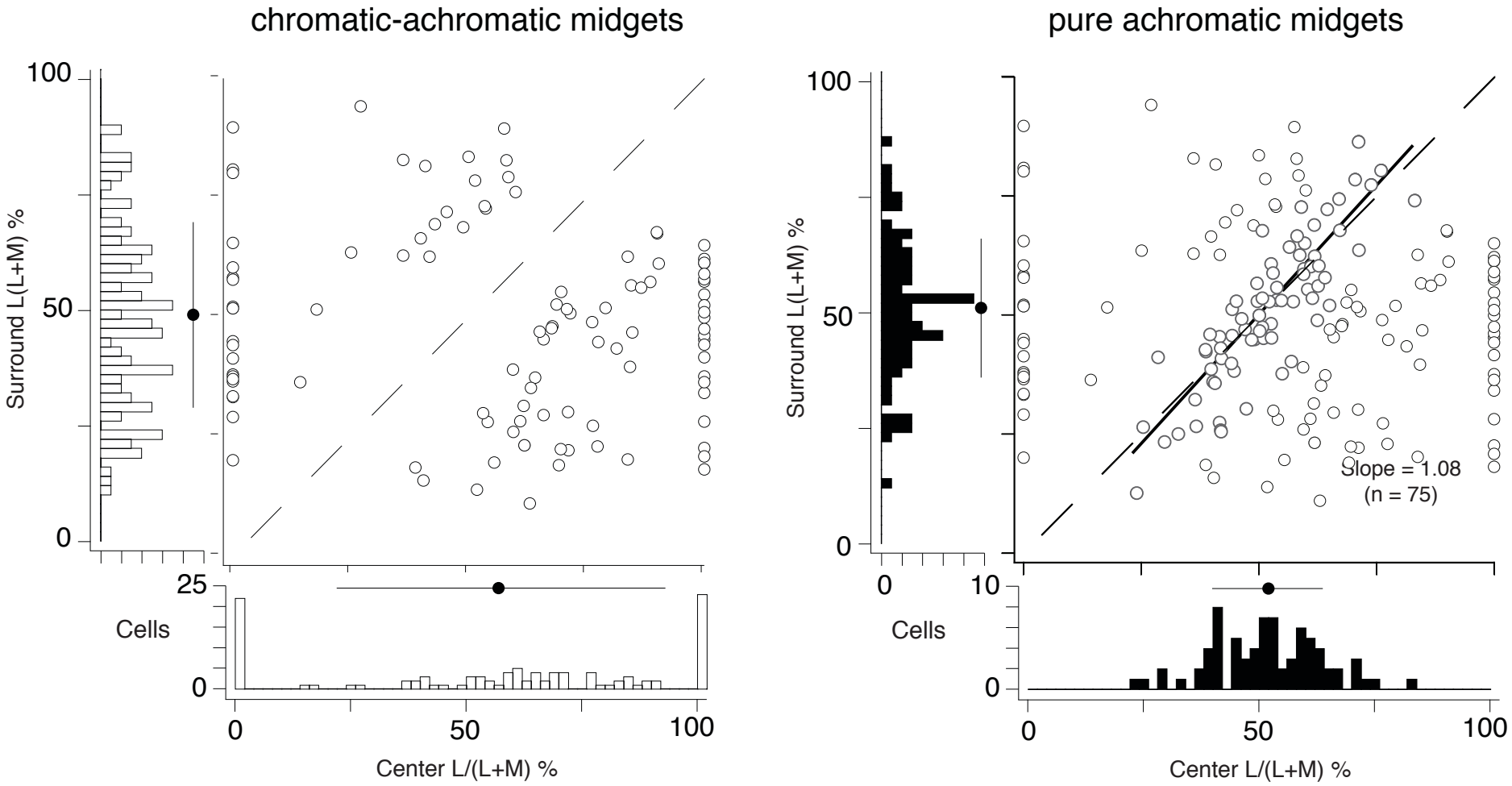

Jo Crook & Dennis Dacey

Cone inputs to the receptive field suggest random wiring

- *inputs to the midget center are variable*
- *all midgets show mixed cone input to the surround*
- *all midgets are achromatic to narrow stimuli*
- *many midgets are purely achromatic*

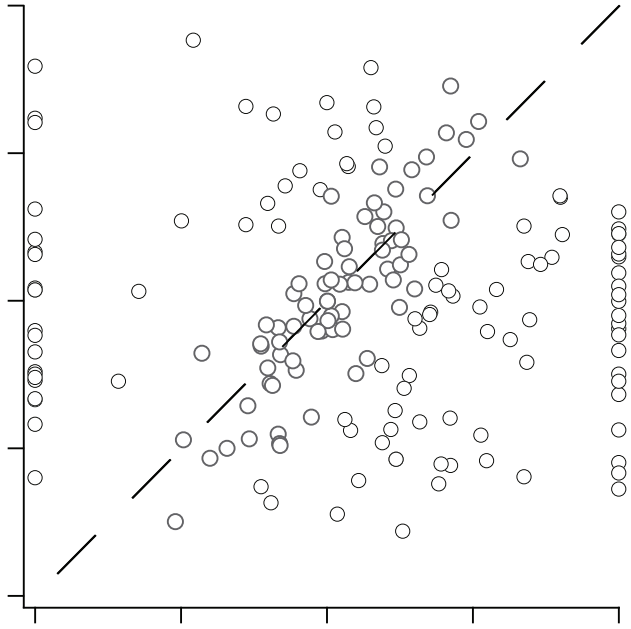

Jo Crook & Dennis Dacey

Primate H1 Horizontal Cell Mosaic

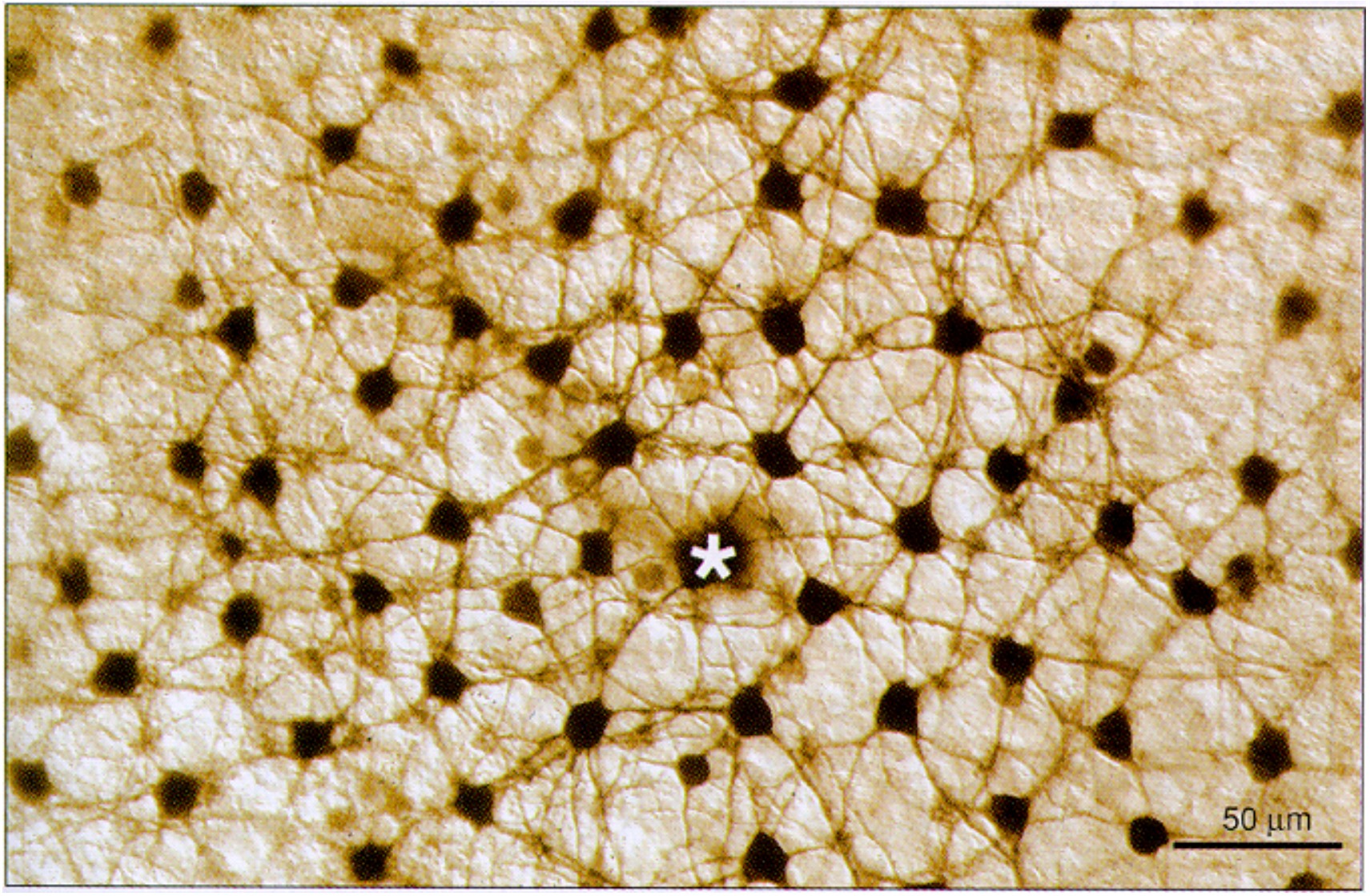

Dacey et al (1996)

As predicted by random-wiring the surround arises by indiscriminate horizontal cell feedback to cones

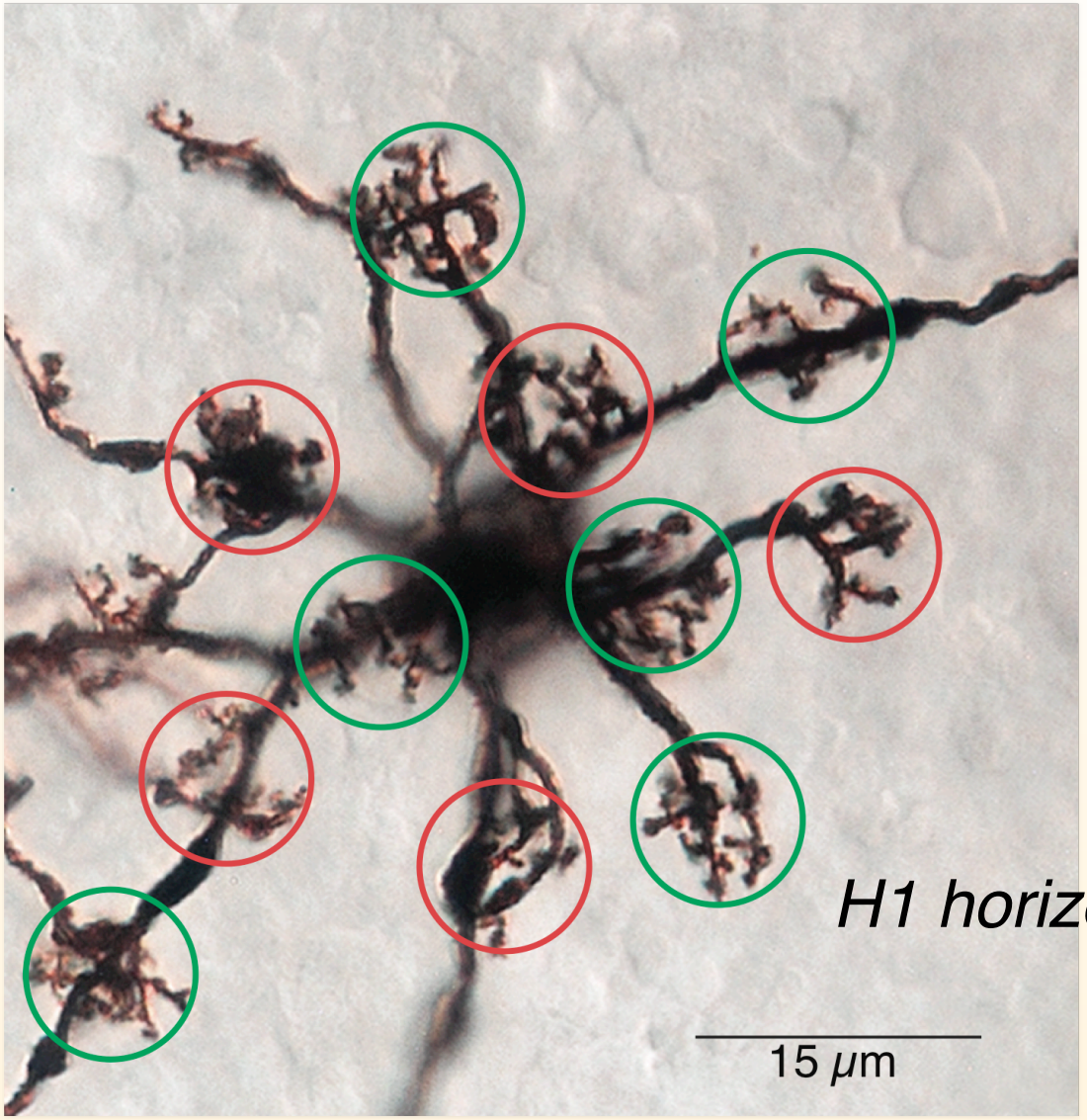

Dacey et al., 1996

Cell-type classification and receptive fields at single-cone resolution.

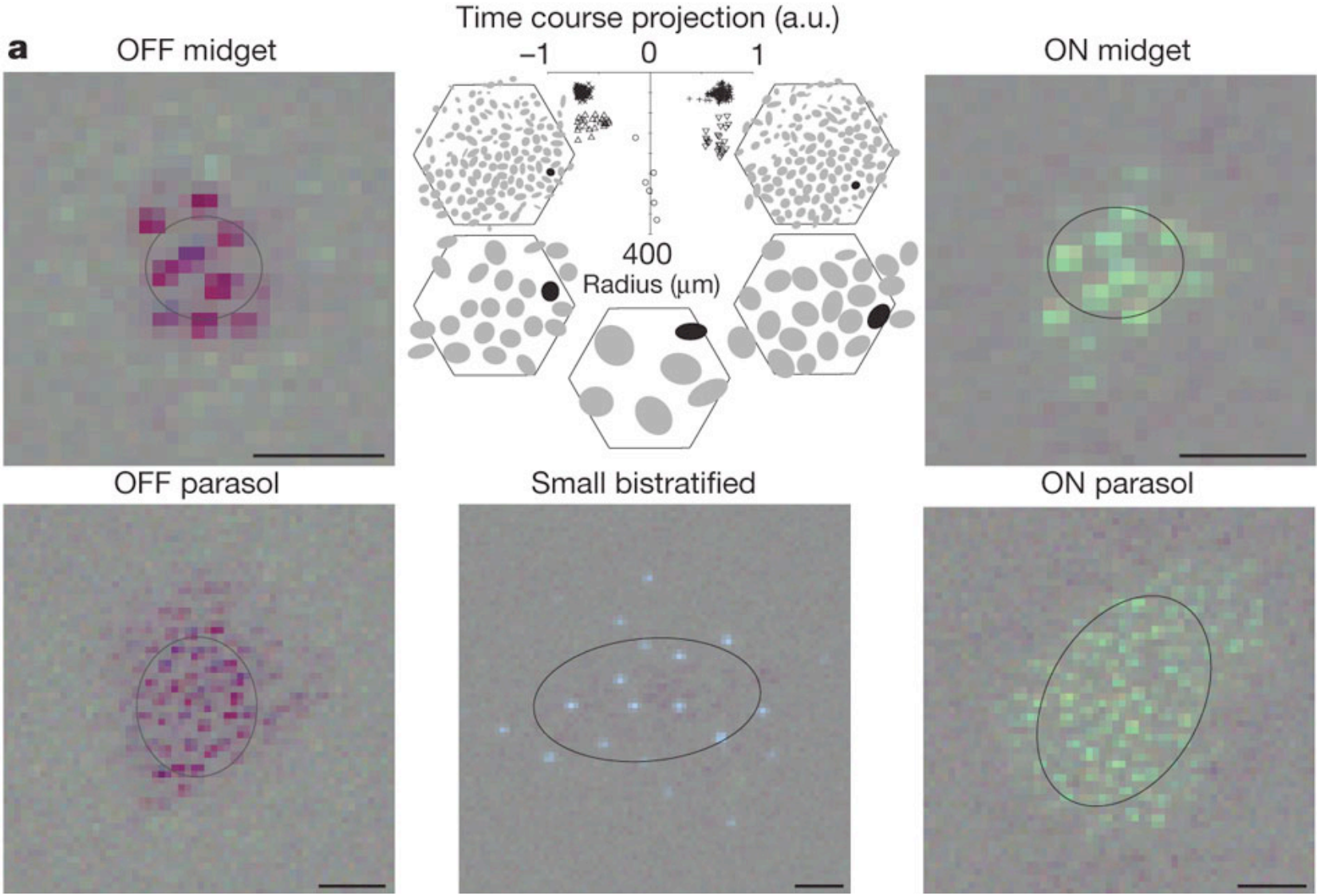

a, Receptive fields of 323 RGCs recorded simultaneously from isolated macaque retina were measured using reverse correlation with white noise stimuli. Centre panel shows receptive-field radius versus first principal component of response time course; clusters reveal distinct cell types. a.u., arbitrary units. Hexagons surrounding centre panel show outline of electrode array and ellipses show Gaussian fits to receptive fields of cells from each cluster. The outer panels show fine-grained spatial receptive-field profiles for highlighted cells. Scale bars, 50 μm

nature
GD Field *et al. Nature* **467**, 673-677 (2010)
doi:10.1038/nature09424

Cone-type identification and inputs to RGCs.

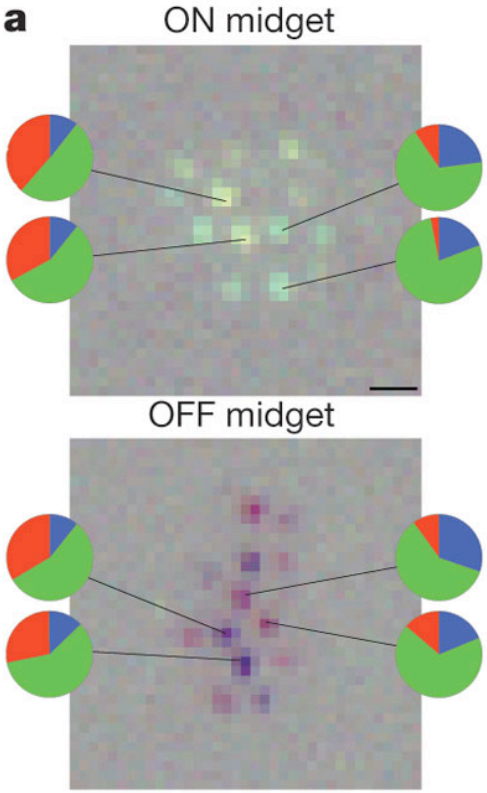

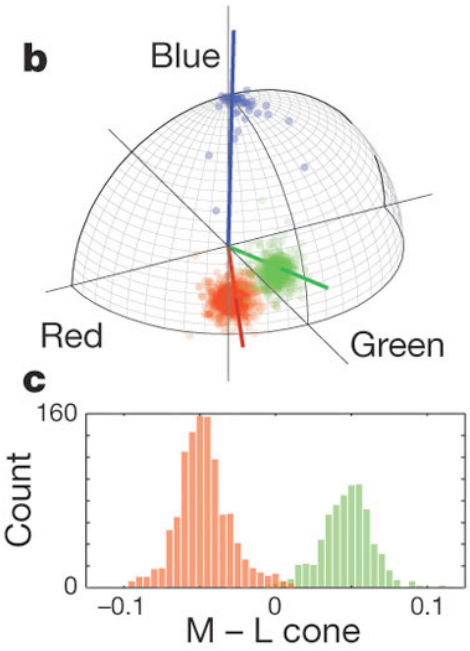

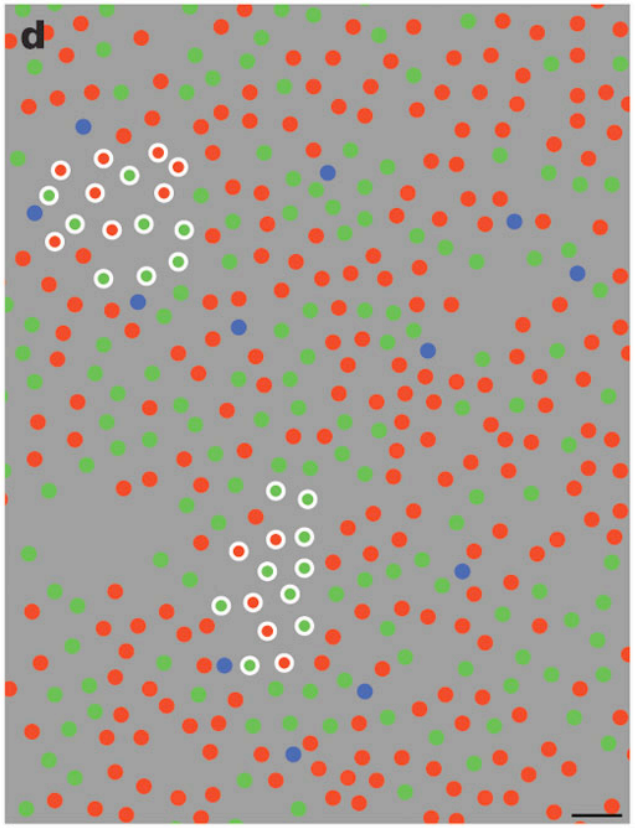

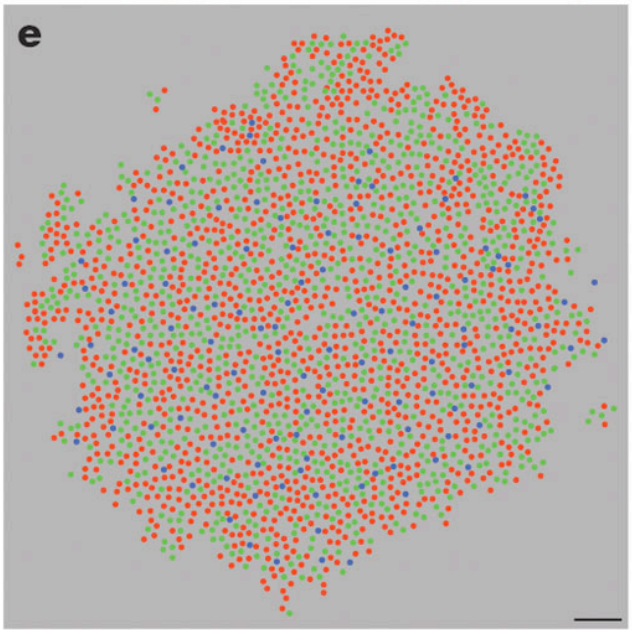

a, The spectral sensitivity of cones providing input to two cells is represented by the relative magnitude of the red, green and blue spike-triggered average values (a.u.) at their locations.

b, For every cone in one recording, these values are shown as points on a sphere. Coloured lines indicate spectral sensitivity of macaque cones. Point colour indicates classification as L (red), M (green), or S (blue).

c, L- and M-cone discriminability quantified by projection along the line joining L- and M-cone loci. Bar colour indicates classification. S cones excluded.

d, Assembled cone mosaic from all RGCs over a region. Cones from **a** are circled.

e, Full mosaic of 2,373 cones from one recording

nature
GD Field *et al. Nature* **467**, 673-677 (2010)
doi:10.1038/nature09424

Full functional sampling of cone lattice by four RGC types

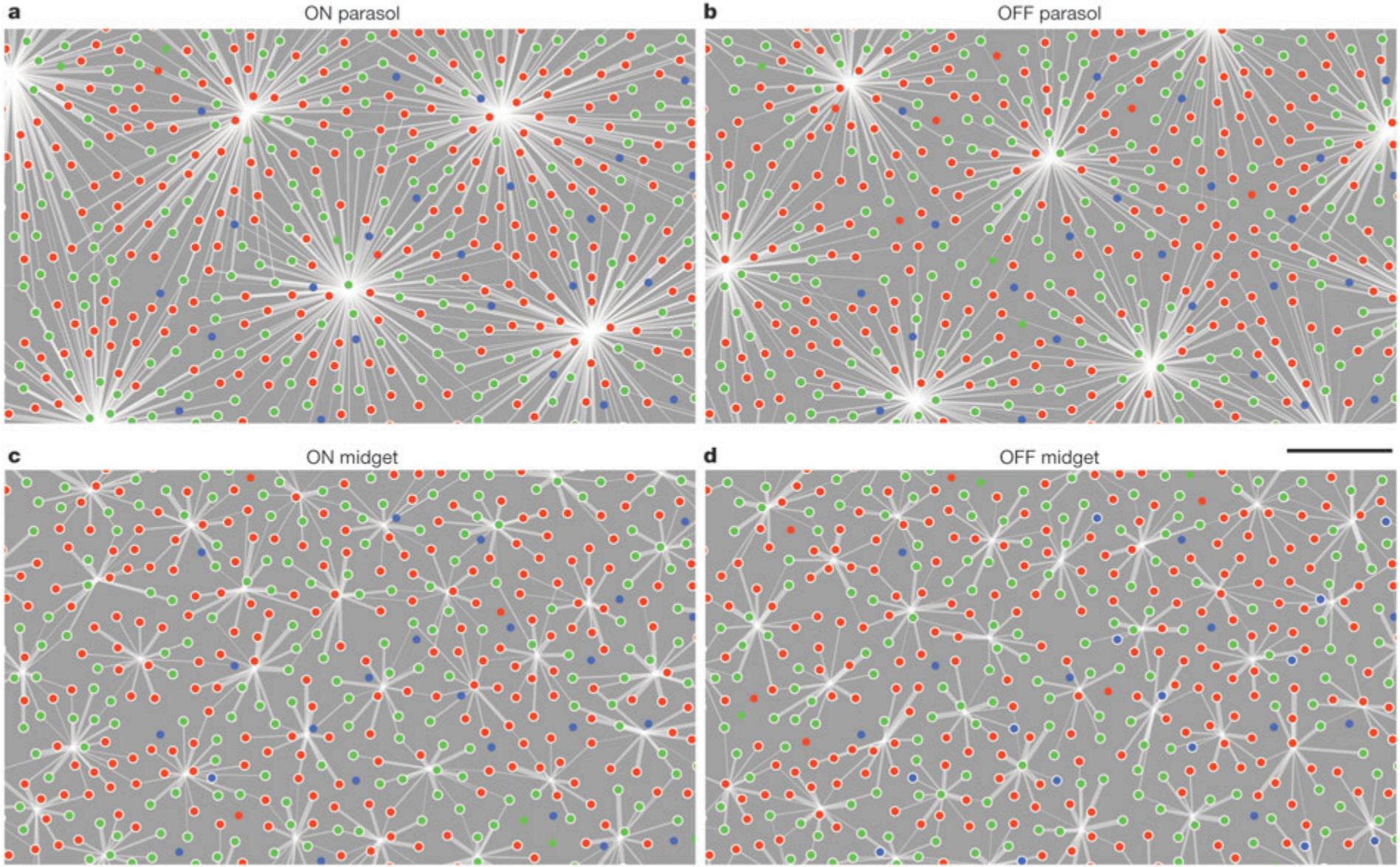

Each panel shows cones identified in a single recording (red, green and blue dots) sampled by receptive-field centres of RGCs of a single type. Cones are identical in all panels. Cones providing input to at least one RGC are highlighted with an annulus. Scale bar, 50 µm.

nature
GD Field *et al. Nature* **467**, 673-677 (2010)
doi:10.1038/nature09424

Cone-type specificity.

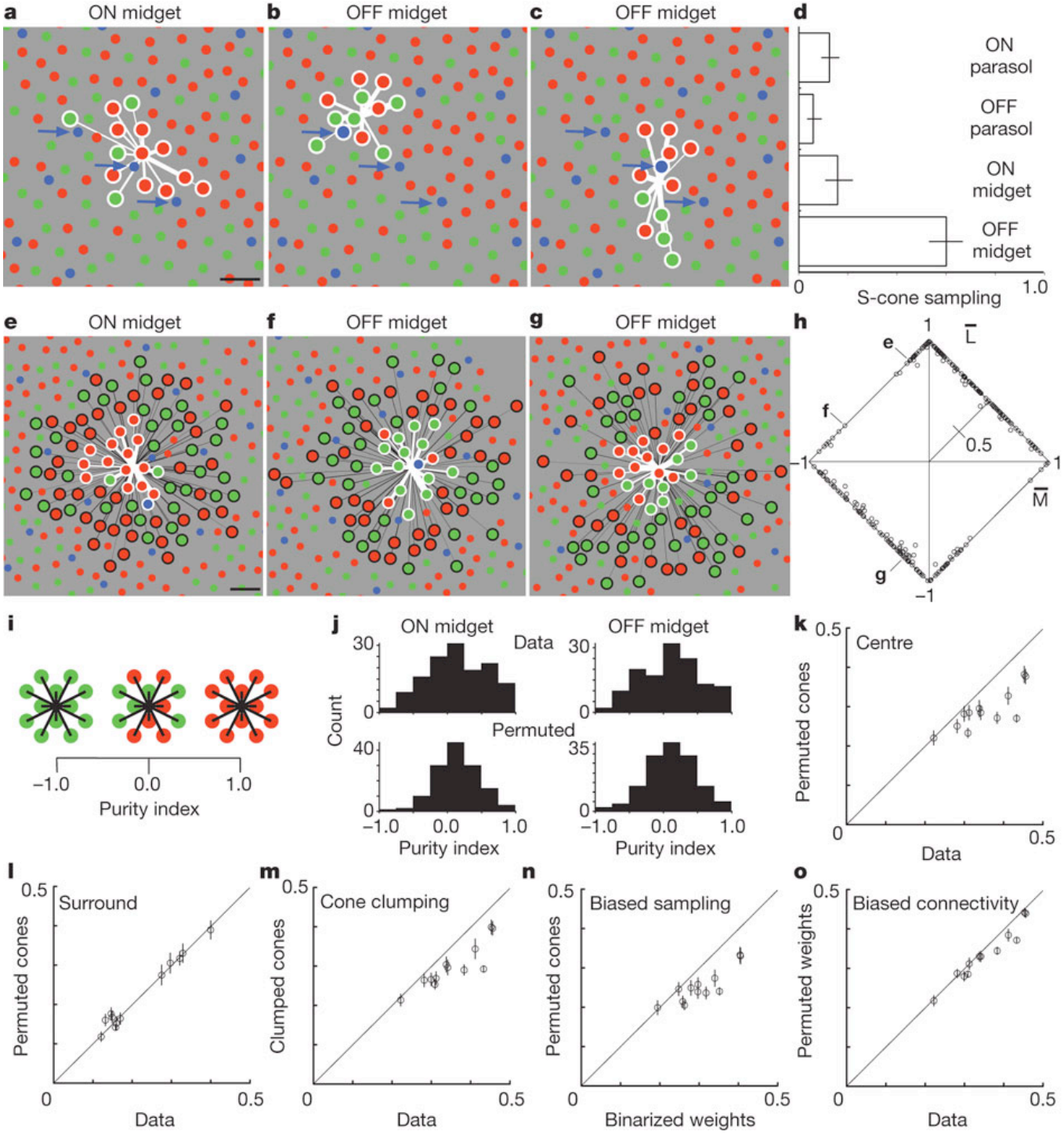

nature
GD Field *et al. Nature* **467**, 673-677 (2010)
doi:10.1038/nature09424

Horace Barlow

Bill Levick

Rabbit Direction-Selective Retinal Ganglion Cells

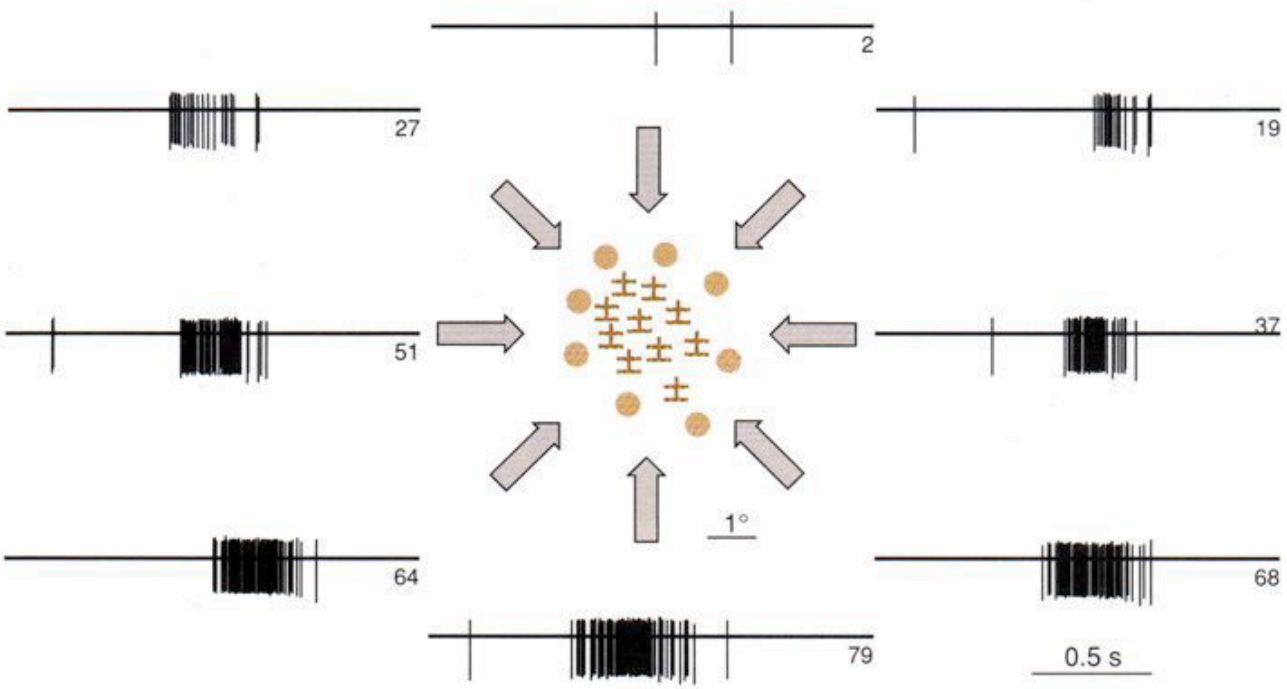

Barlow et al (1964)

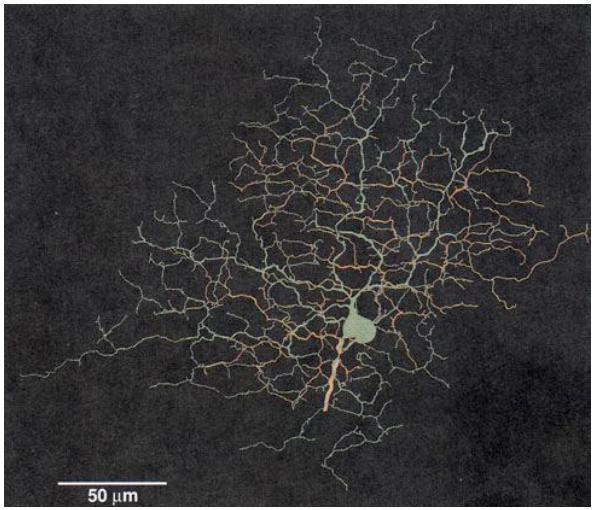

Amthor et al (1989)

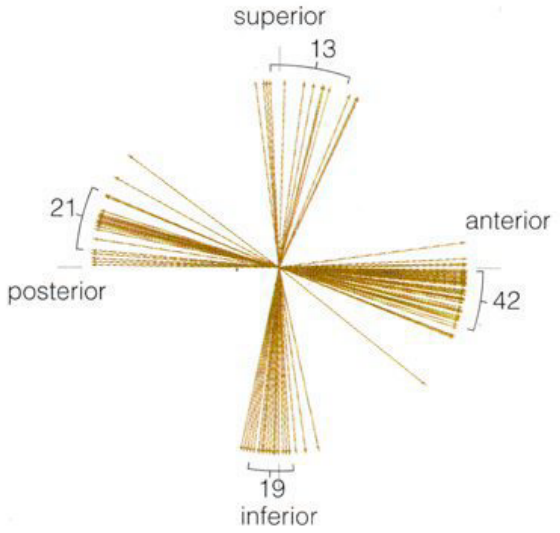

Oyster (1968)

Rabbit Starburst Amacrine Cells

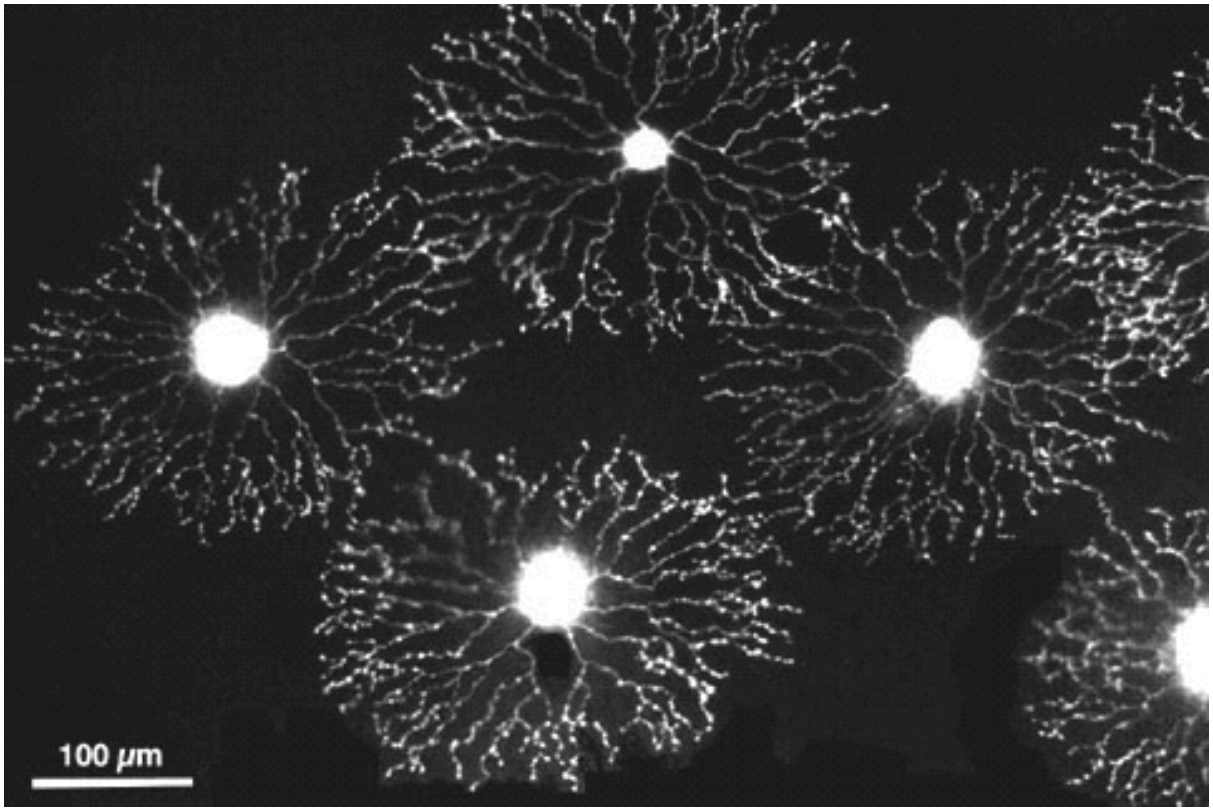

Vaney (1990)

Receptive field properties of on-off directionally selective ganglion cells

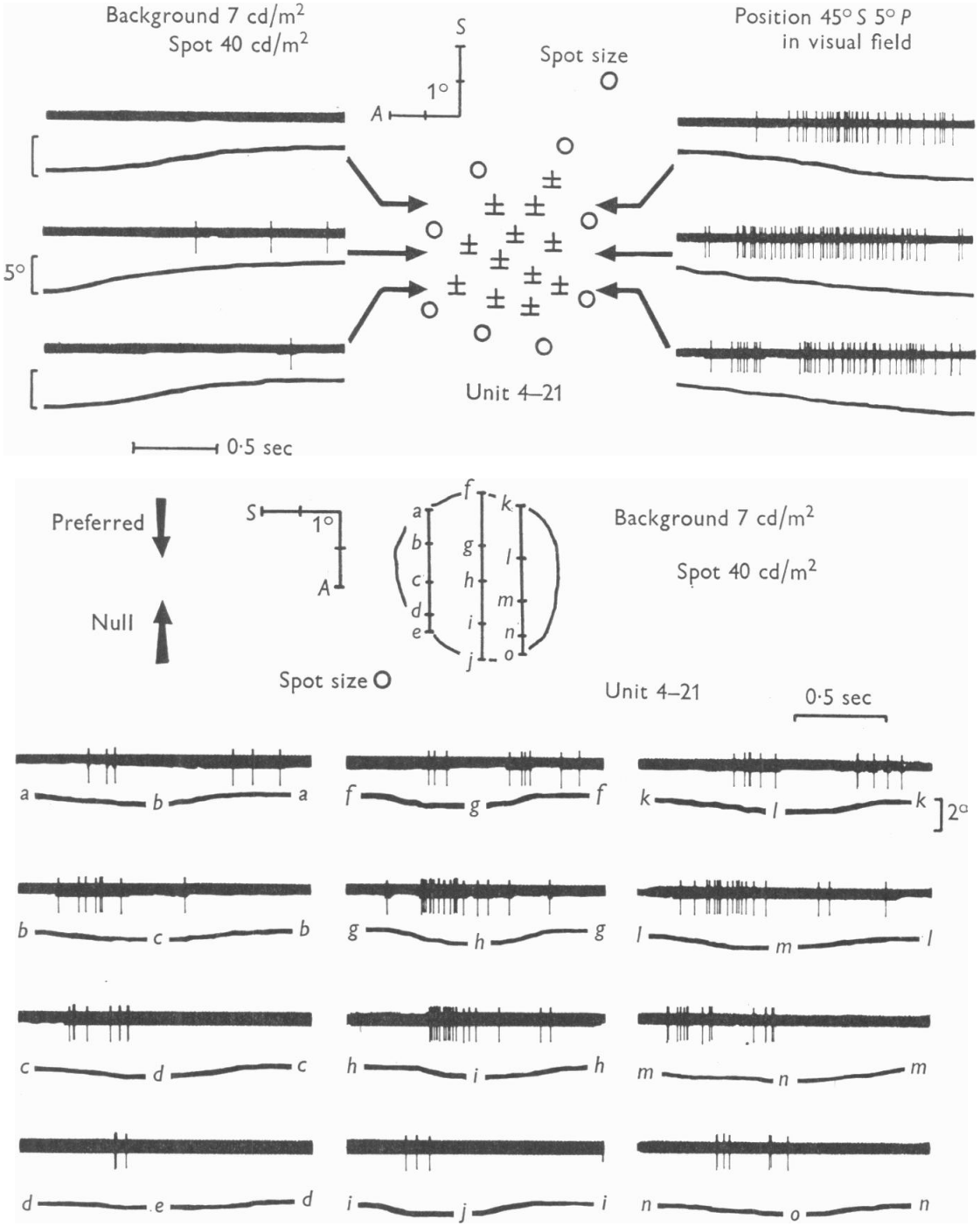

Barlow & Levick, 1965

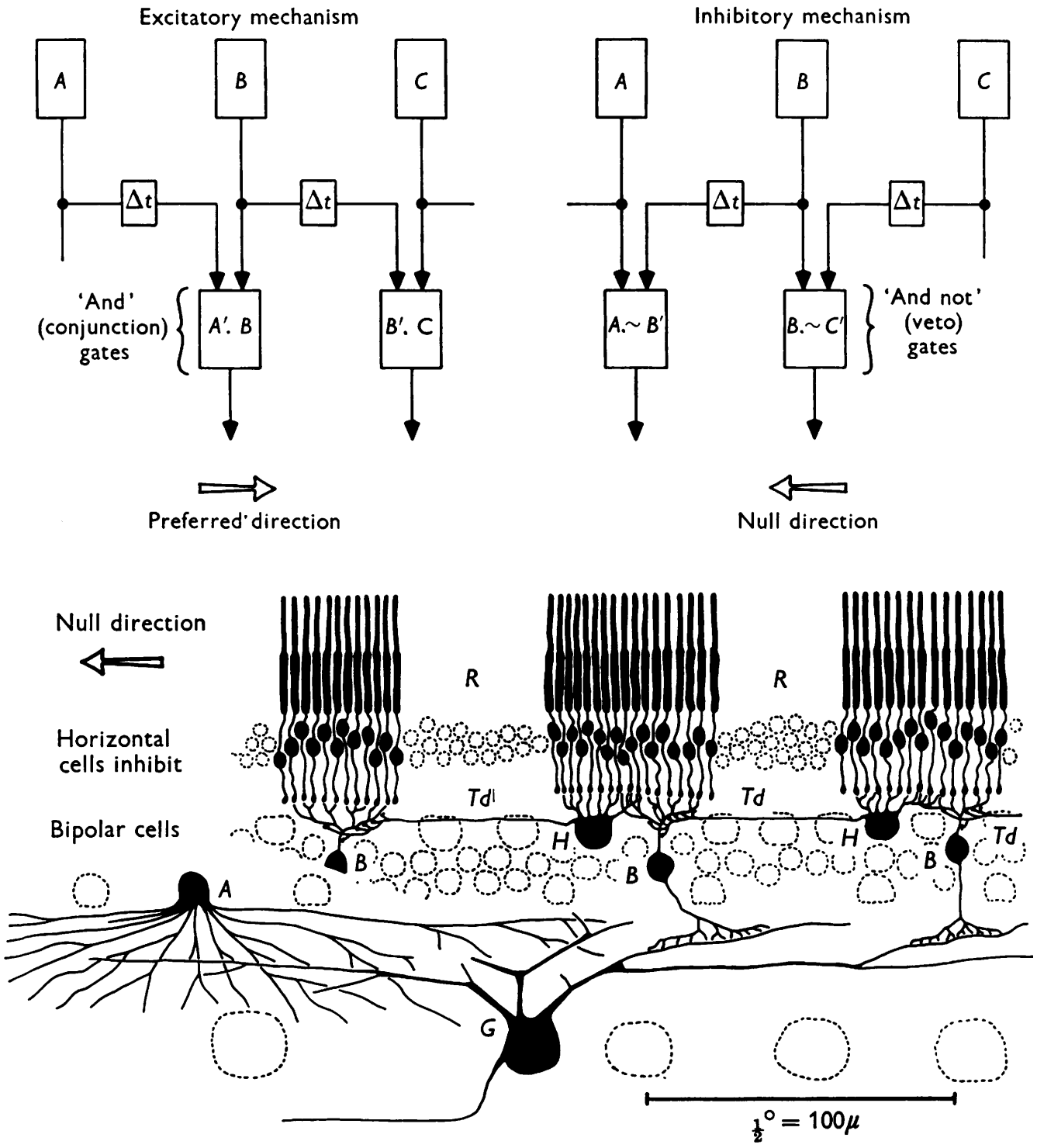

Barlow & Levick, 1965

Receptive field properties of on-off directionally selective ganglion cells

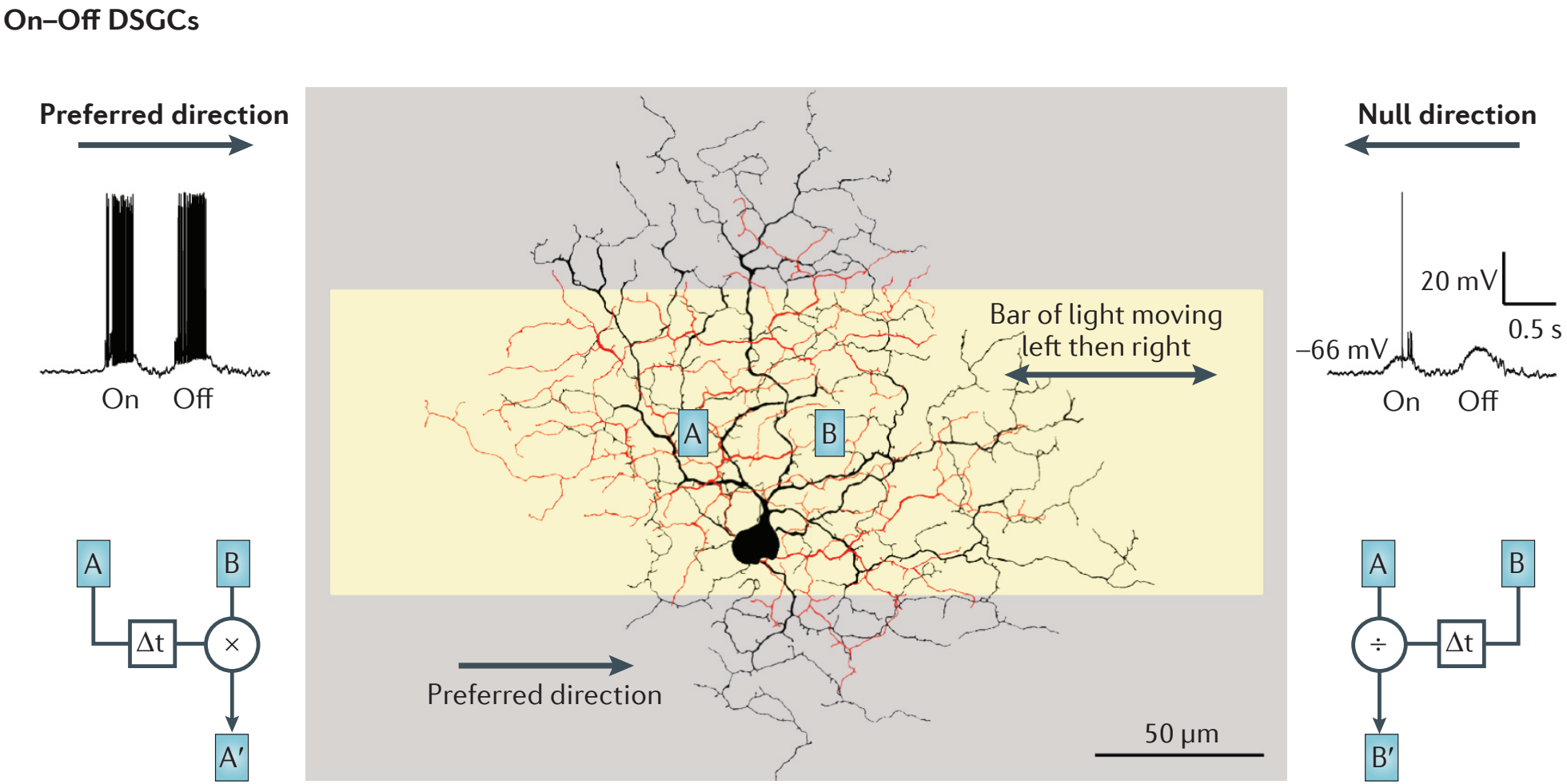

Vaney, et al, 2012

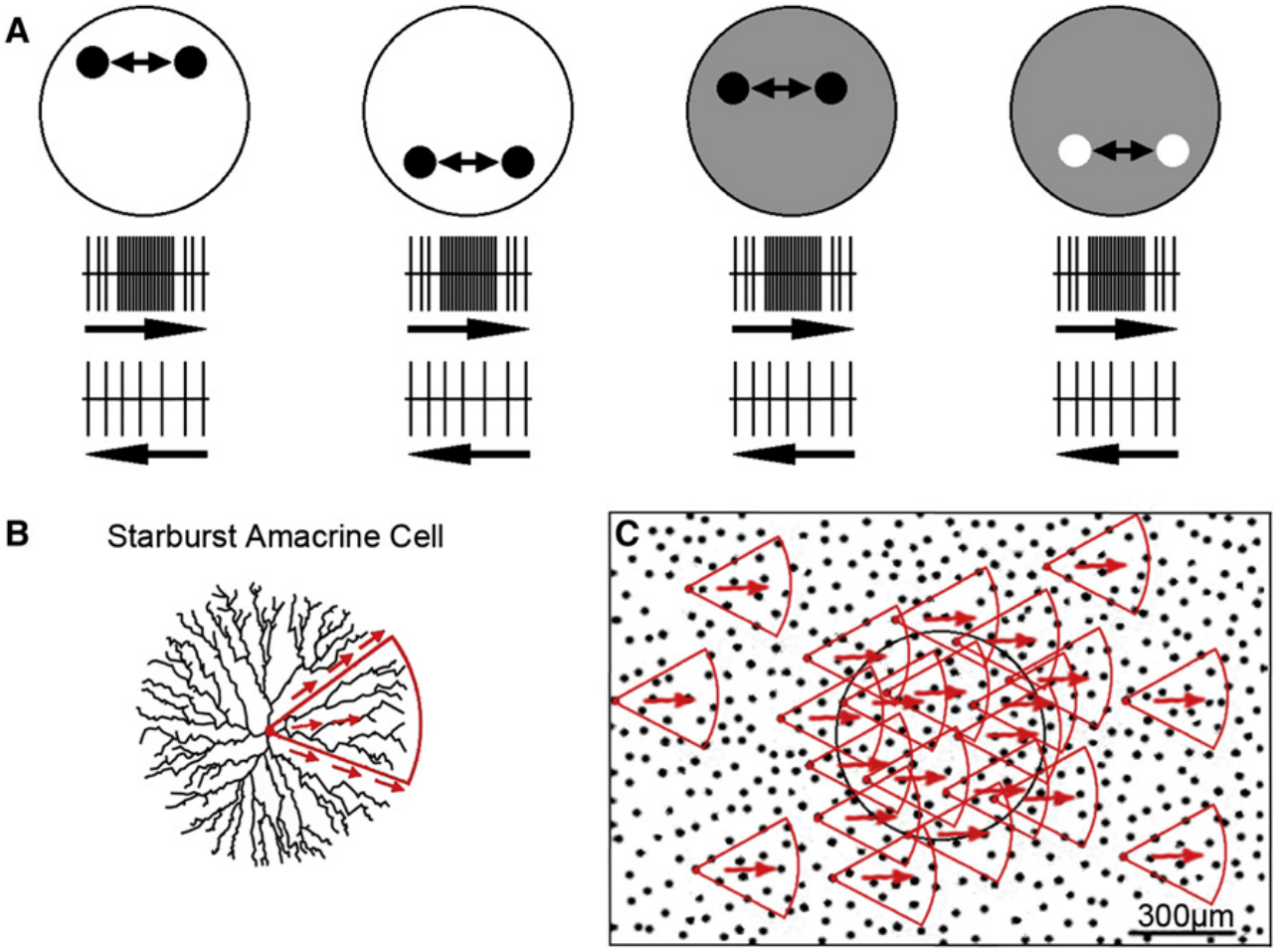

Figure 7. The Cardinal Features of the ON-OFF Direction-Selective Cell, and the Mechanism by Which Direction Selectivity Is Created

(A) The cell can discriminate the direction of motion of small stimuli falling within its receptive field (large circle), and it does not matter where within the field the small stimulus falls—there is a local subunit that is direction selective.

(B and C) The fundamental mechanism of direction selectivity. (B) Shows the dendritic arbor of a starburst amacrine cell. A sector of the arbor (outlined in red) is (1) an independent functional unit, electrically separate from the rest of the cell, and (2) directionally polarized, such that it releases GABA when the stimulus moves in one direction—left to right in this example—and not in others. (C) Starburst sectors pointing in a single direction (red) selectively synapse upon dendrites of an ON-OFF DS ganglion cell (outlined by the black circle). In this example, they would provide inhibition when the stimulus moves from left to right. This cell would thus have a preferred direction for movement right-to-left and a null direction for movement left-to-right. The sectors are smaller than the dendritic field, thus accounting for the ganglion cell's ability to discriminate small movements within the field. Other sectors of the starburst cell, pointing in other directions, would contact other direction selective ganglion cells; those cells would prefer different directions of stimulus movement.

Masland, 2012

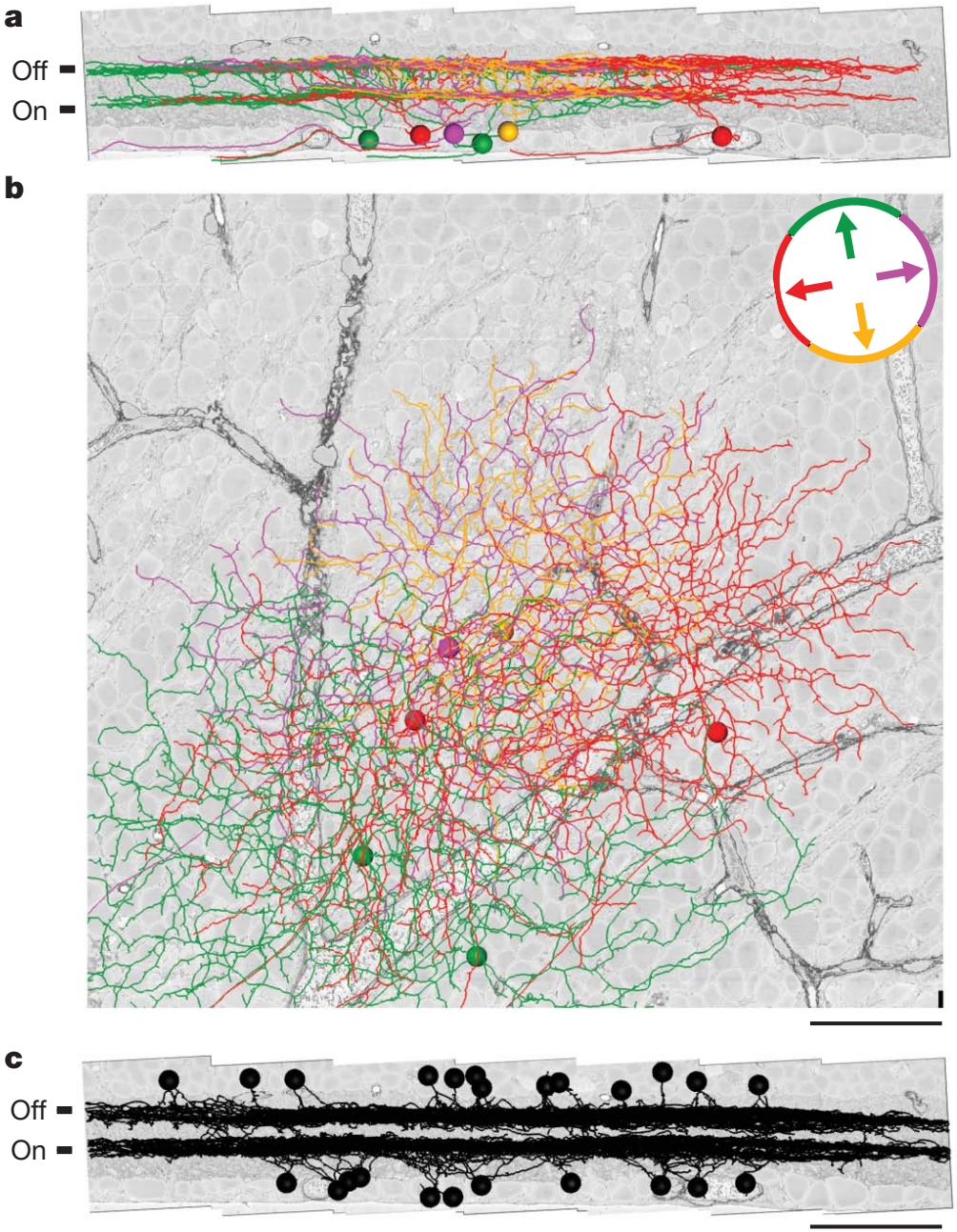

Figure 2 | Skeleton reconstructions of DSGCs and SACs. **a**, **b**, DSGCs, colour-coded by preferred direction (inset), projected parallel to (**a**) and norma to (**b**) the plane of the retina. Note bi-stratification in the inner plexiform layer **c**, Parallel projections of 24 SACs (11 On SACs, 13 Off SACs, black). Scale bar are 50 μm.

Briggman et al, 2011

Asymmetric interactions with starburst amacrine circuits

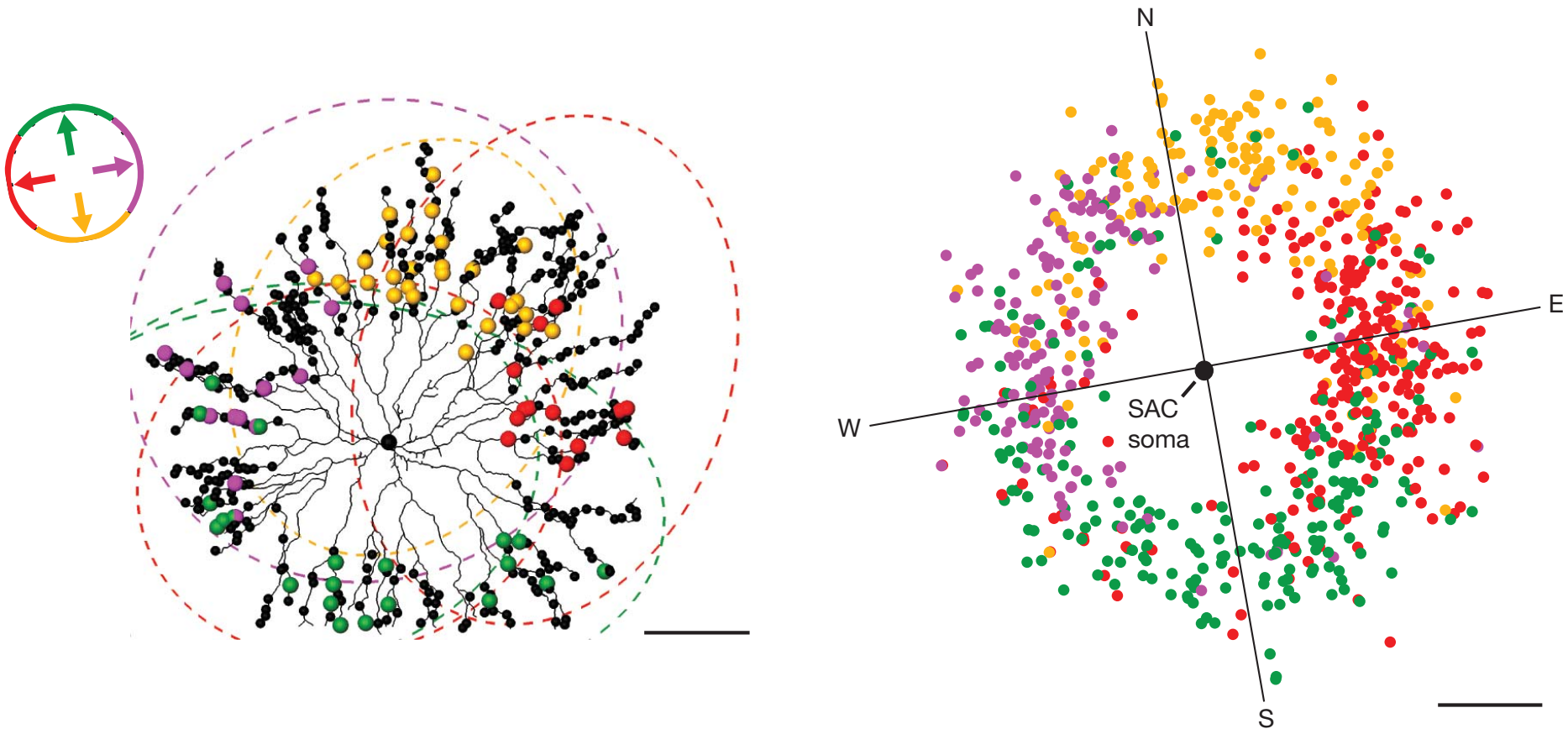

Figure 4 | Specificity of SAC outputs. **a**, An Off SAC (black skeleton), with varicosities indicated by black dots. DSGC dendritic trees are indicated by colour-coded dashed ellipses. Synapses are colour-coded by the preferred direction of the postsynaptic DSGC. **b**, Output synapse locations ($n = 831$ synapses) relative to SAC somata from all 24 SACs. Scale bars are 50 µm.

Briggman et al, 2011

Direction-specific interactions with starburst amacrine circuits

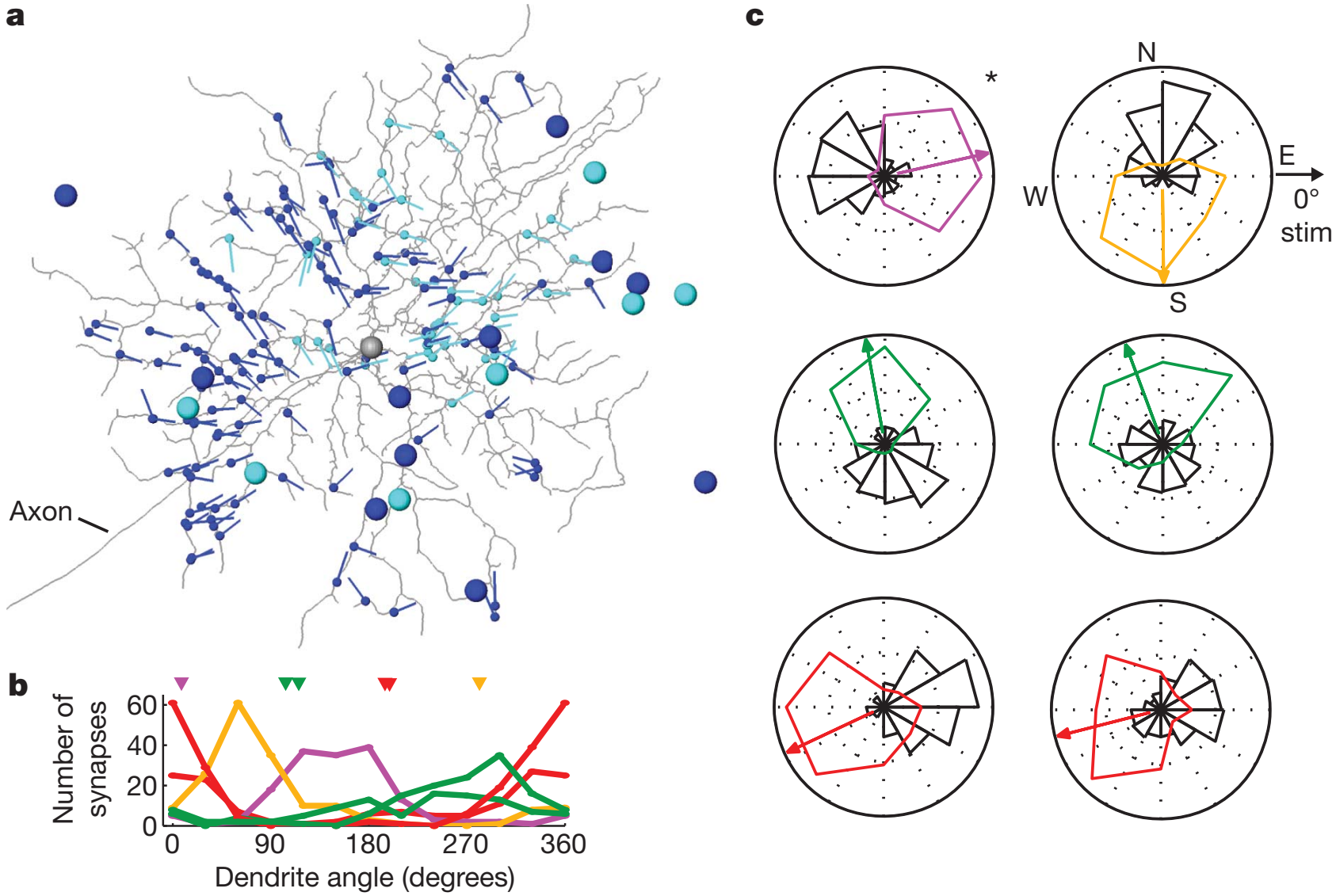

Figure 5 | Specificity of DSGC inputs. **a**, DSGC (grey skeleton) and the connected On and Off SAC somata (large cyan and blue circles, respectively) and associated SAC input synapses (smaller cyan and blue circles) from 18 SACs. **b**, The distribution of all SAC dendrite angles (θ_{dendr}) for each of the six DSGCs; θ_{dendr} is defined by the vectors (cyan and blue lines in **a**) oriented from SAC somata to synapse location. Triangle markers indicate the preferred direction for each DSGC. **c**, Polar histograms of θ_{dendr} (black, plotted as the square root of θ_{dendr} frequencies) together with the DSGC tuning curves (as in Fig. 1). Asterisk denotes the DSGC shown in **a**.

Briggman et al, 2011

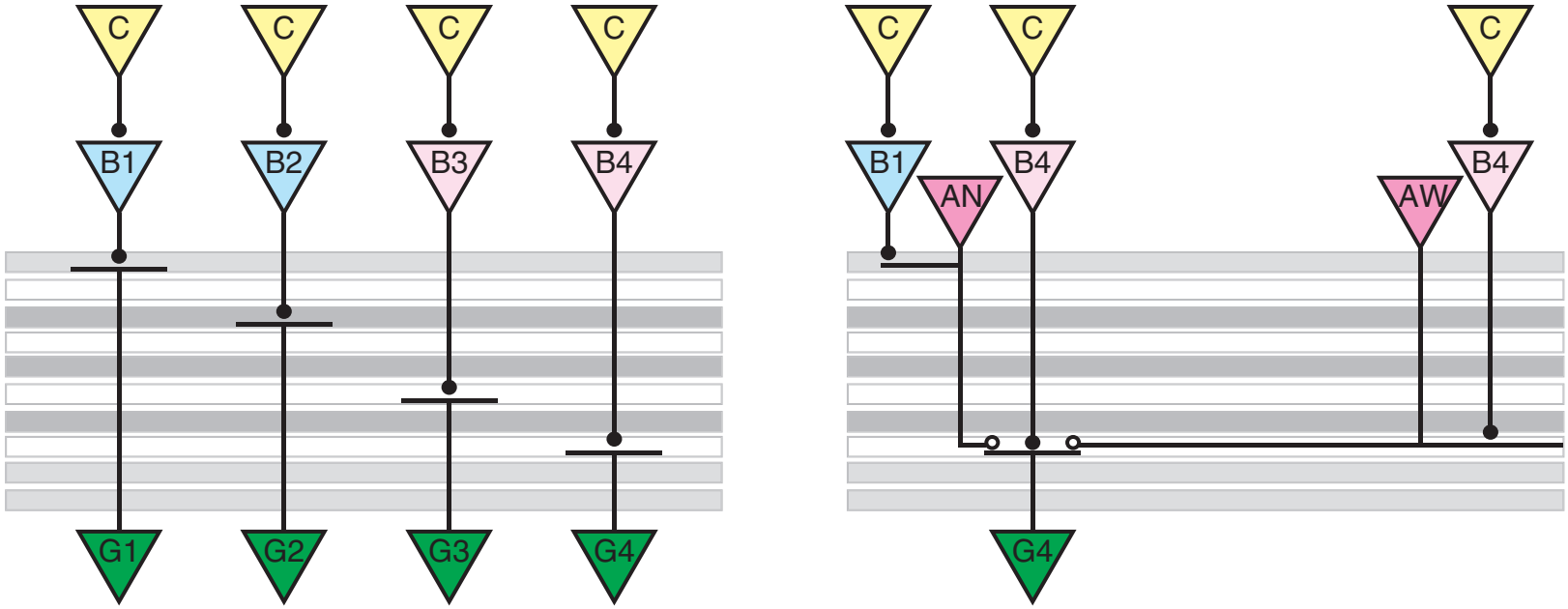

FIGURE 13.4 Retinal features are stacked in the inner retina. (Left) Bipolar cell terminals and ganglion cell dendrites are laid down in different strata of the IPL. (Right) Some amacrine cells (AN) are narrow and tall; their inputs and outputs are in different strata. Other amacrine cells (AW) are wide and flat, with long processes in one stratum; these cells carry information across the local circuits of the same mosaic.

Roska & Meister, 2014

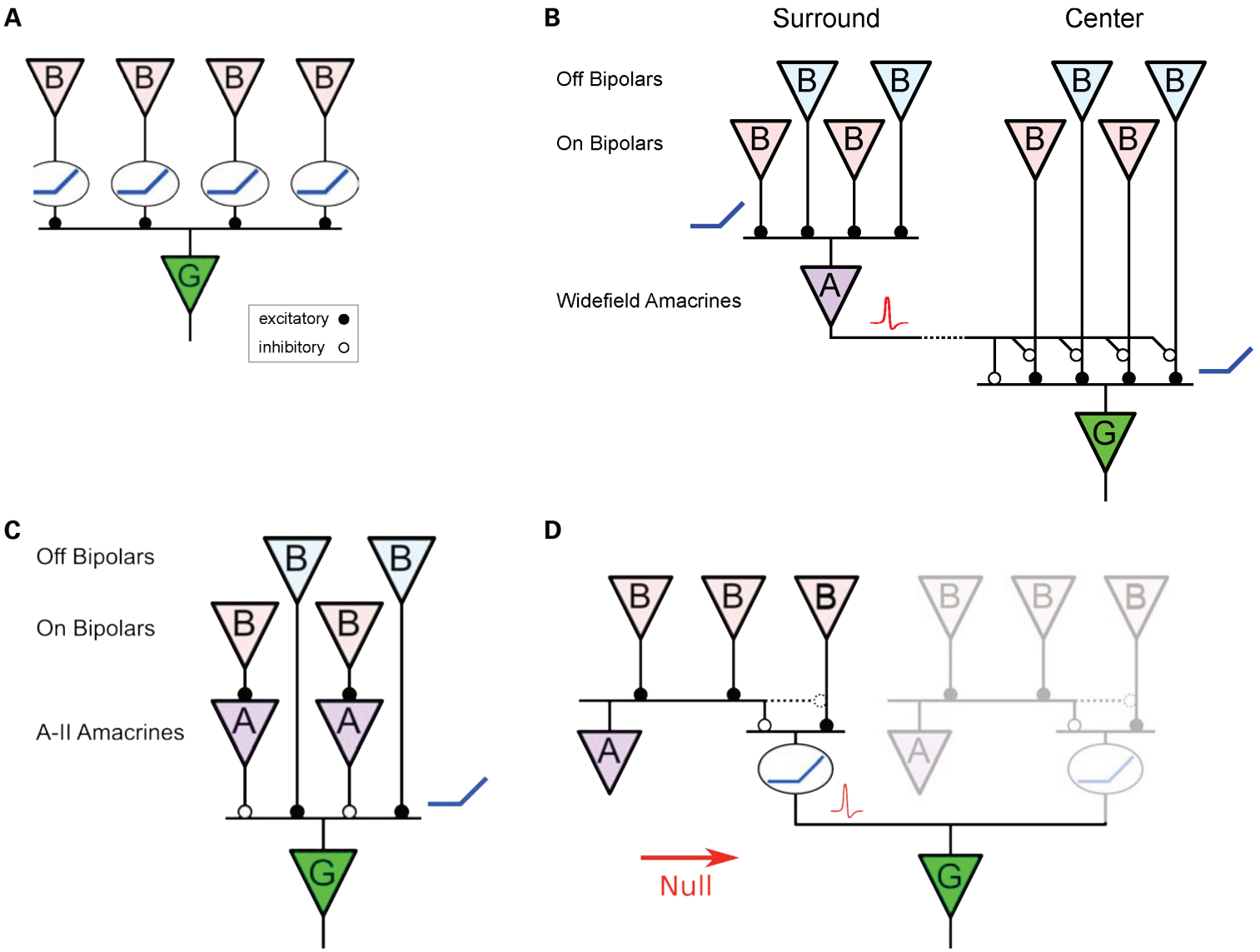

FIGURE 13.7 Retinal circuits leading to different feature detector ganglion cells. (A) The Y-type ganglion cell. This ganglion cell collects excitation from many bipolar cells. The bipolar cell synapses are rectifying: At baseline the release rate of transmitter is low, so depolarization increases transmitter release, but hyperpolarization has little or no effect. In subsequent panels, this rectifying quality is assumed for all bipolar cell synapses. (B) The object-motion-sensitive cell. Note that the ganglion cell pools over both ON and OFF bipolars, but this process is gated by the action of a wide-field amacrine cell. (C) The looming detector. Again there is pooling over ON and OFF channels, but with opposite sign because of an interposed narrow amacrine cell. (D) The direction-selective ganglion cell. The asymmetric interaction that defines the null direction occurs between the dendrite of a starburst amacrine cell and local bipolar cells. An additional threshold nonlinearity arises from spike generation within the dendritic tree of the ganglion cell.

Roska & Meister, 2014

Hierarchy of Visual Processing

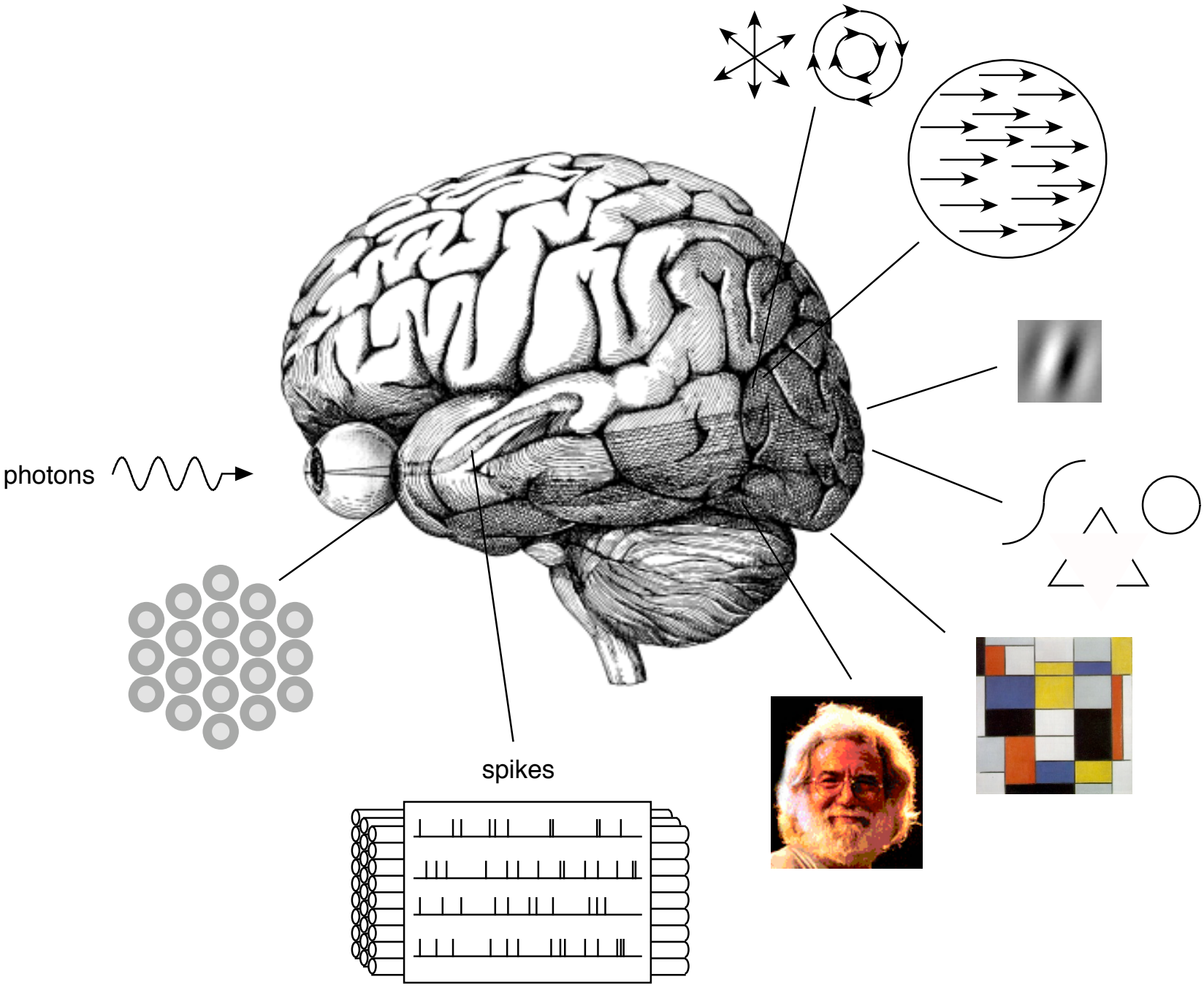

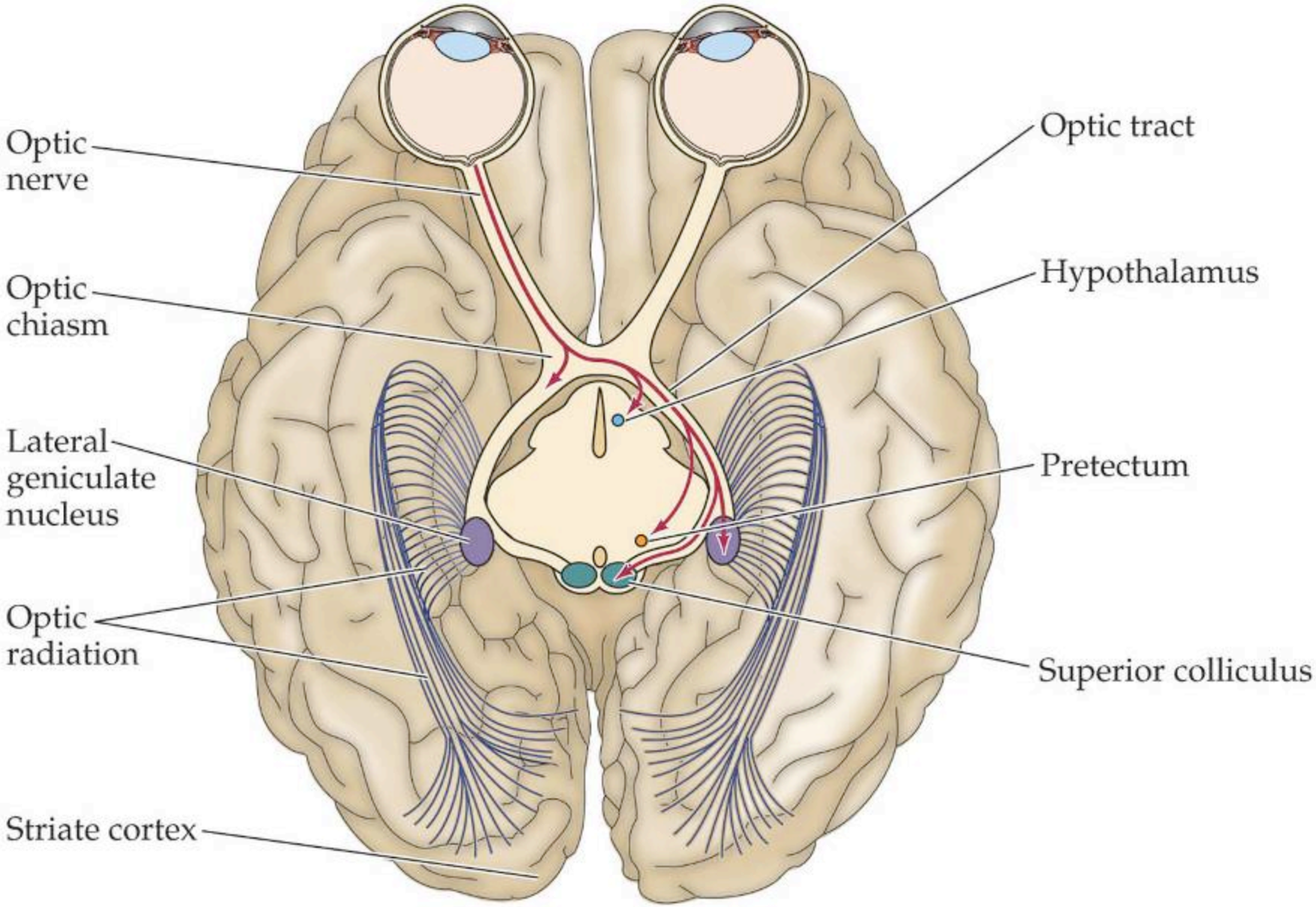

NEUROSCIENCE, Third Edition, **Figure 11.2**

Projections of the retina

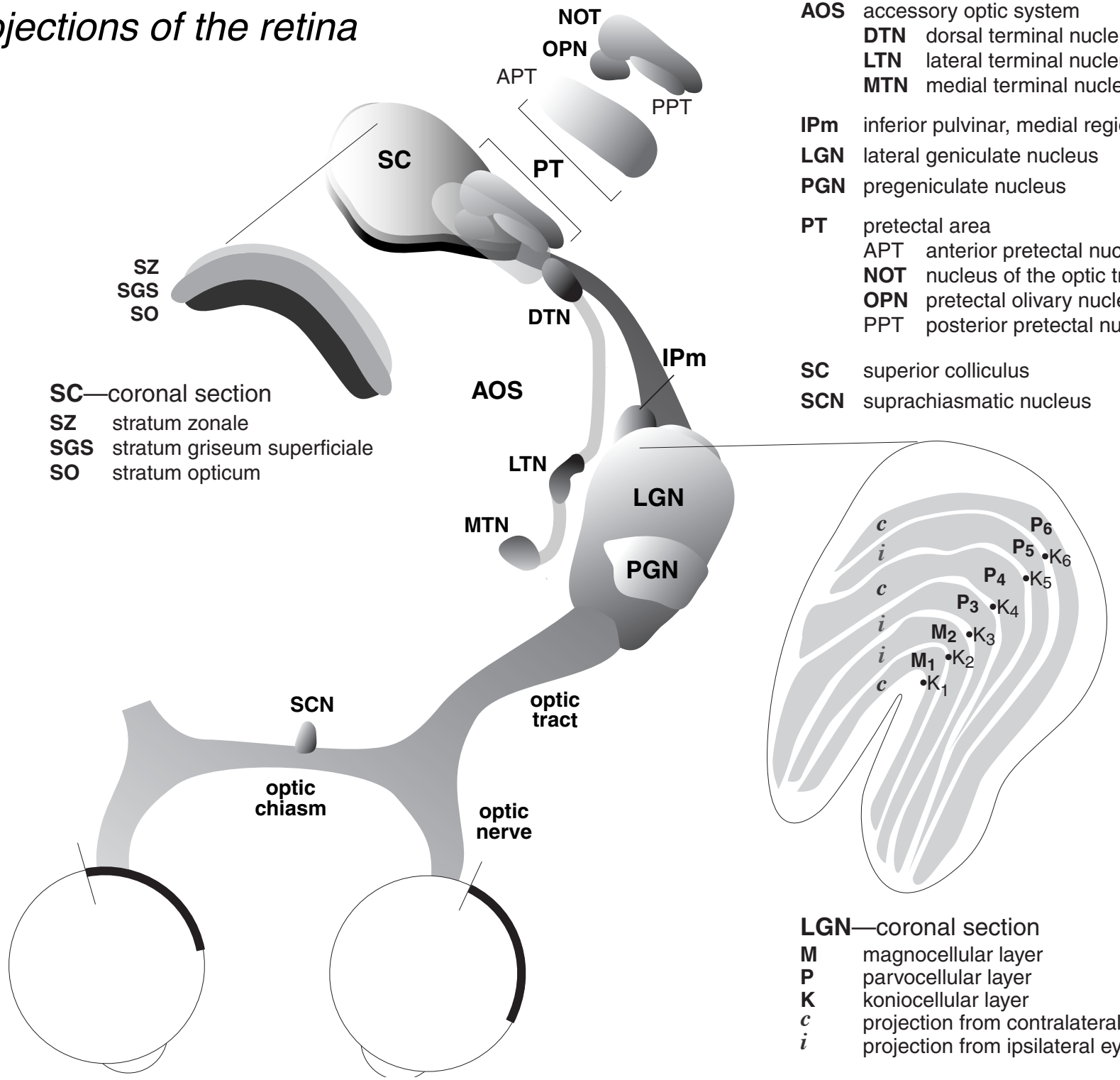

AOS accessory optic system
- **DTN** dorsal terminal nucleus
- **LTN** lateral terminal nucleus
- **MTN** medial terminal nucleus

IPm inferior pulvinar, medial region

LGN lateral geniculate nucleus

PGN pregeniculate nucleus

PT pretectal area
- APT anterior pretectal nucleus
- **NOT** nucleus of the optic tract
- **OPN** pretectal olivary nucleus
- PPT posterior pretectal nucleus

SC superior colliculus

SCN suprachiasmatic nucleus

SC—coronal section
- **SZ** stratum zonale
- **SGS** stratum griseum superficiale
- **SO** stratum opticum

LGN—coronal section
- **M** magnocellular layer
- **P** parvocellular layer
- **K** koniocellular layer
- *c* projection from contralateral eye
- *i* projection from ipsilateral eye

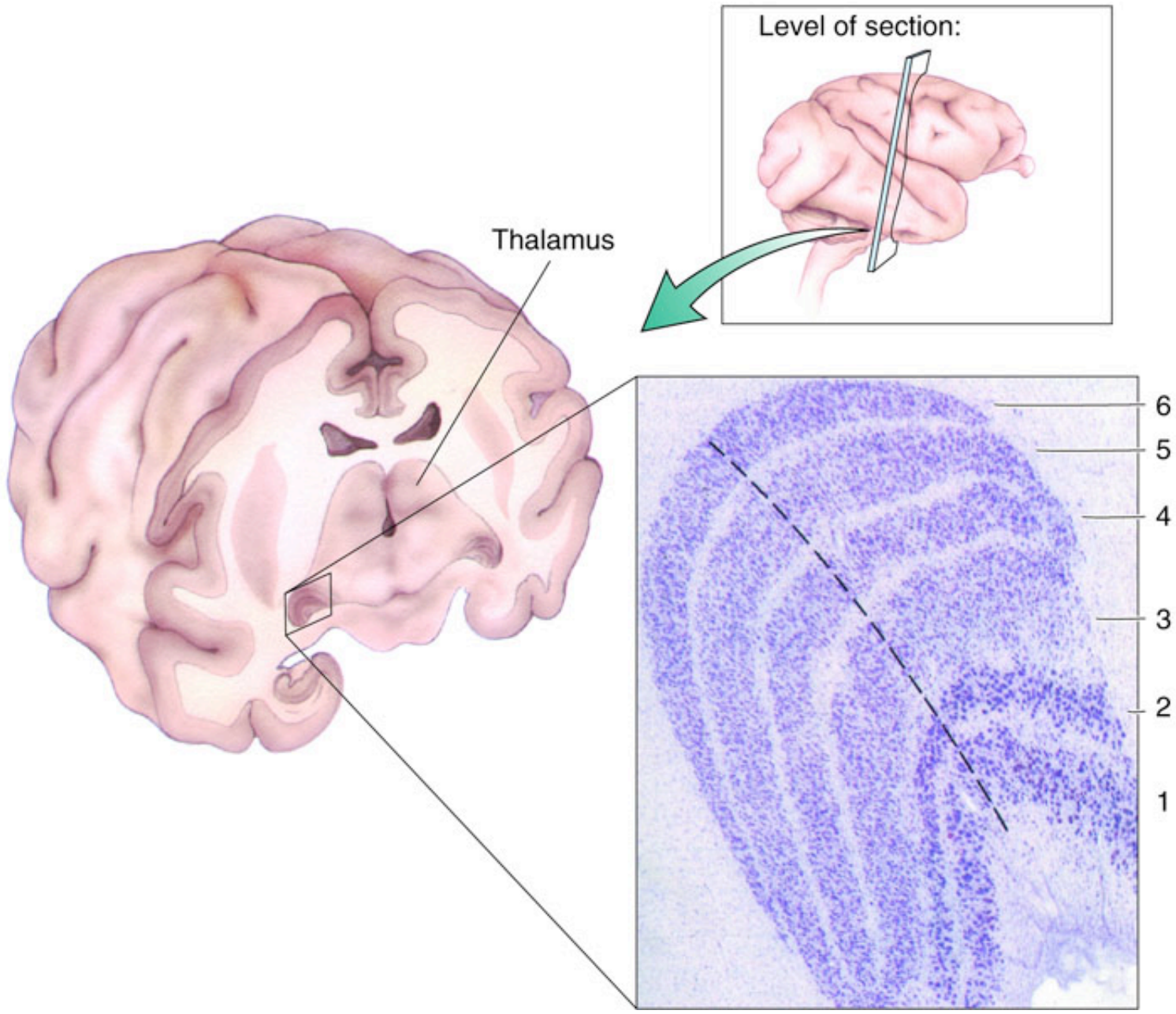
Level of section:
Thalamus
6
5
4
3
2
1

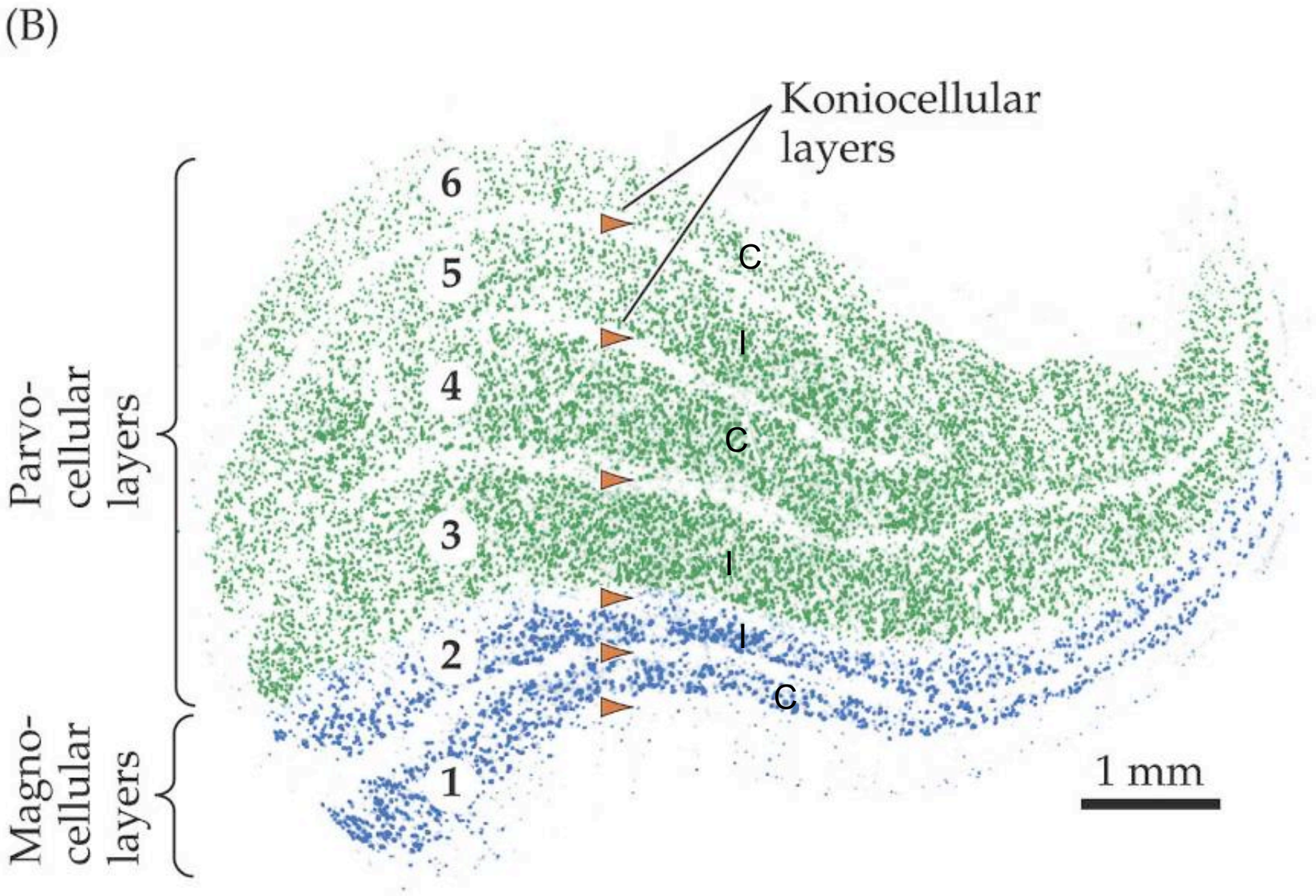

NEUROSCIENCE, Third Edition, Figure 11.14 (Part 2)

Figure 1. Laminar organization of the LGN in five different primates: galago, squirrel monkey, macaque monkey, chimpanzee, and human

In each, neurones in the magnocellular, parvocellular and koniocellular streams occupy distinct laminae. In the galago, magnocellular neurones occupy layers 1 and 2, parvocellular neurones occupy layers 3 and 6, and koniocellular neurones occupy layers 4 and 5 and the intercalated zones. In the squirrel monkey, macaque monkey, chimpanzee and human, magnocellular neurones occupy layers 1 and 2, parvocellular neurones occupy layers 3, 4, 5 and 6, and koniocellular neurones occupy the intercalated layers below and between each of the magnocellular and parvocellular layers. Although the squirrel monkey lacks clear intercalated zones between the parvocellular layers, koniocellular neurones have been reported between the layers.

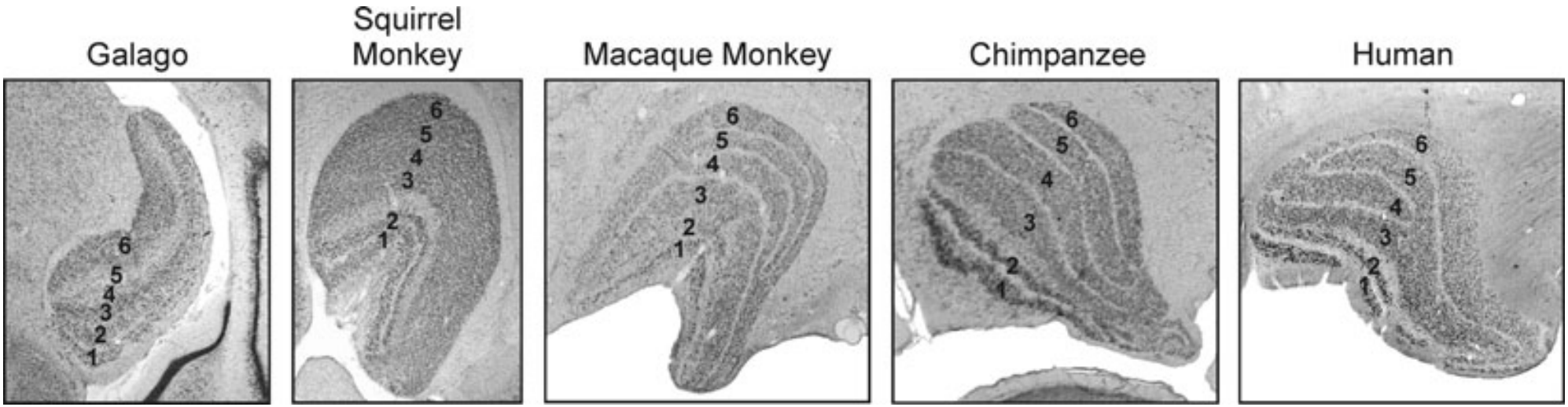

Briggs & Usrey, 2011

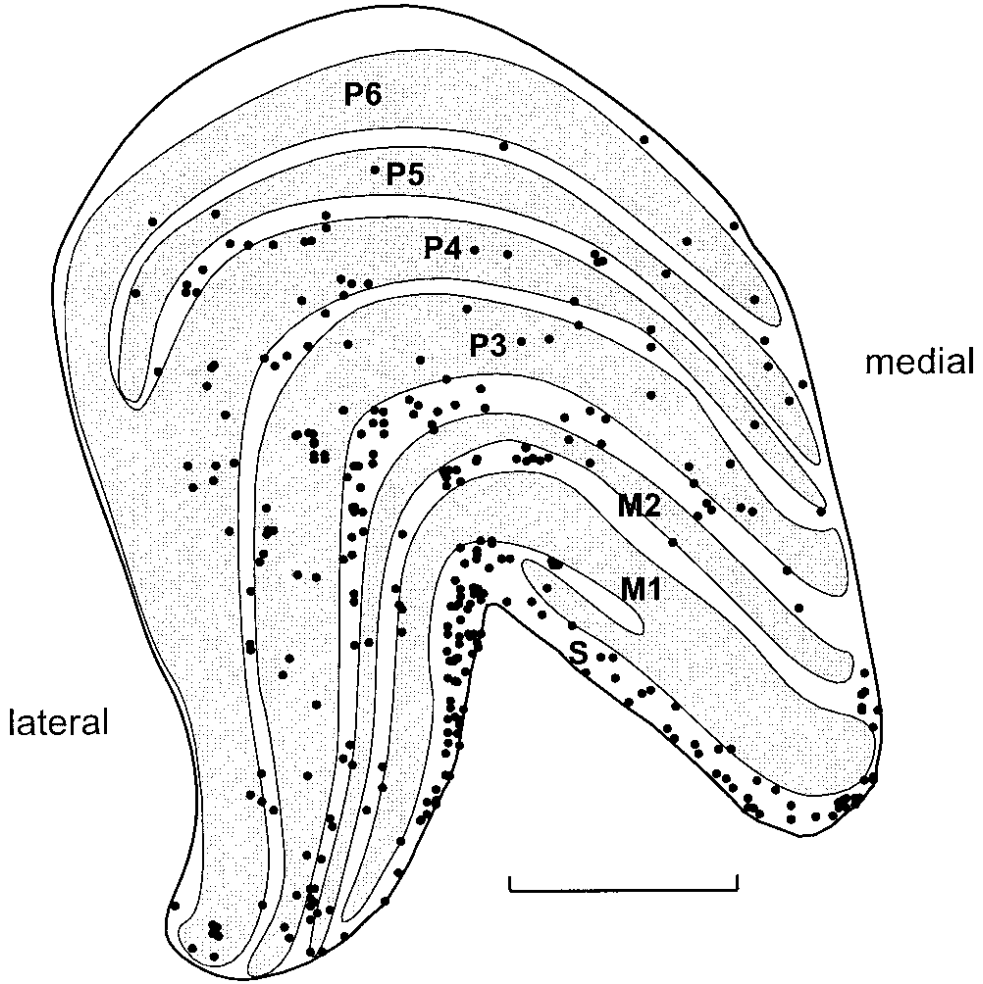

Fig. 2. Charting of calbindin D-28K (Cal) -immunoreactive neurons within a coronal section through the dorsal lateral geniculate nucleus (dLGN) in case A. Each dot corresponds to one immunoreactive neuron. P, parvocellular layers; M, magnocellular layers; S, S layers. Scale bar = 1 mm.

Monkey LGN

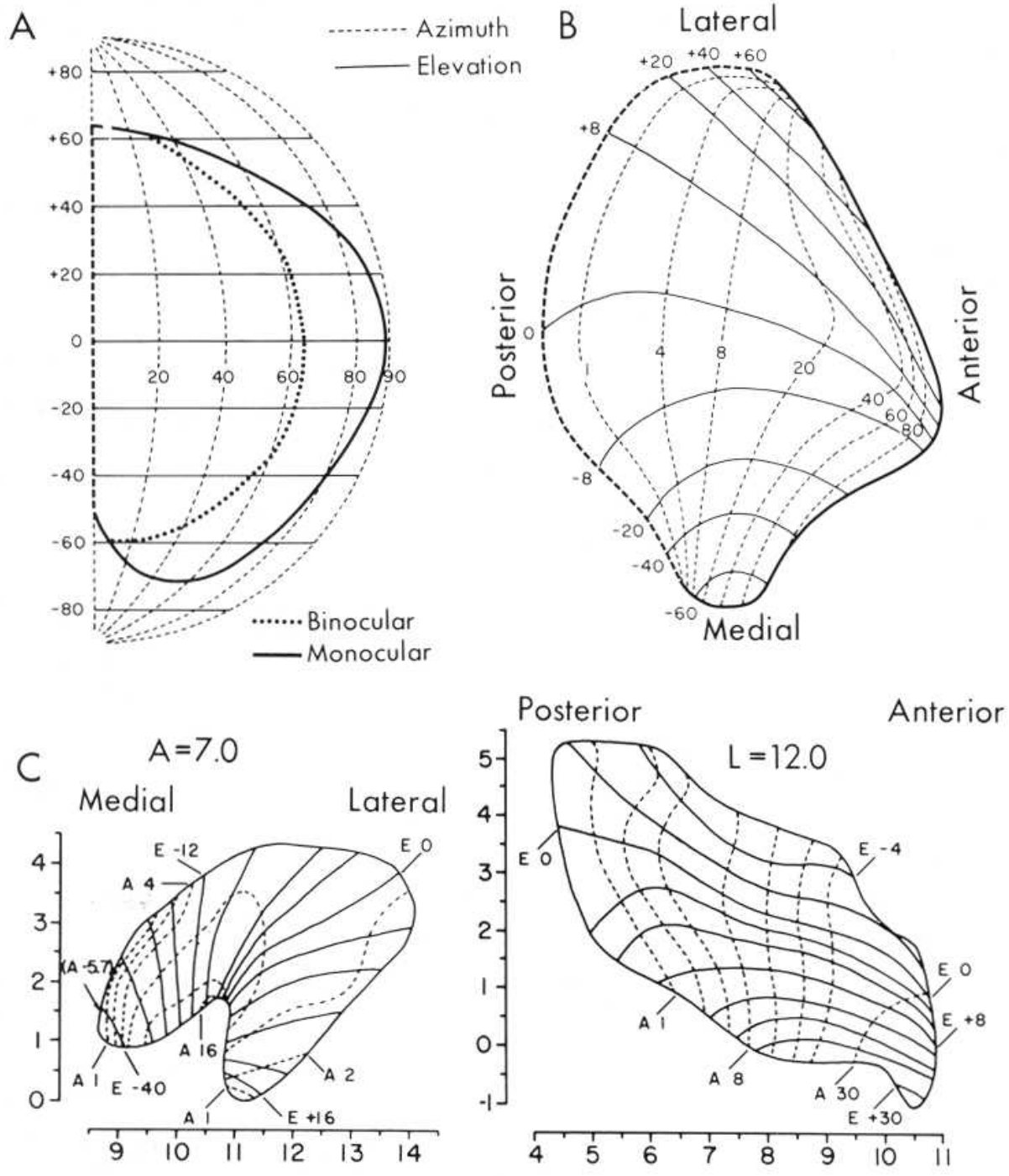
A
Azimuth
Elevation
+80
+60
+40
+20
0
-20
-40
-60
-80
20
40
60
80
90
Binocular
Monocular
B
Lateral
+20
+40
+60
+8
0
-8
-20
-40
-60
4
8
20
40
60
80
Posterior
Anterior
Medial
C
A=7.0
Medial
Lateral
E -12
E 0
A 4
(A -5.7)
A 16
A 2
A 1
E -40
A 1
E +16
9
10
11
12
13
14
Posterior
Anterior
L=12.0
E 0
E -4
E 0
E +8
A 1
A 8
A 30
E +30
4
5
6
7
8
9
10
11

Responses in the retina and the LGN are more or less the same

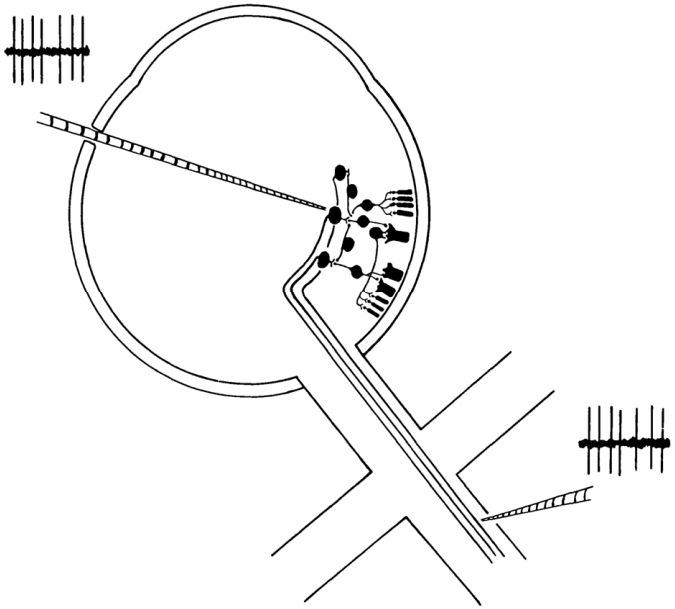

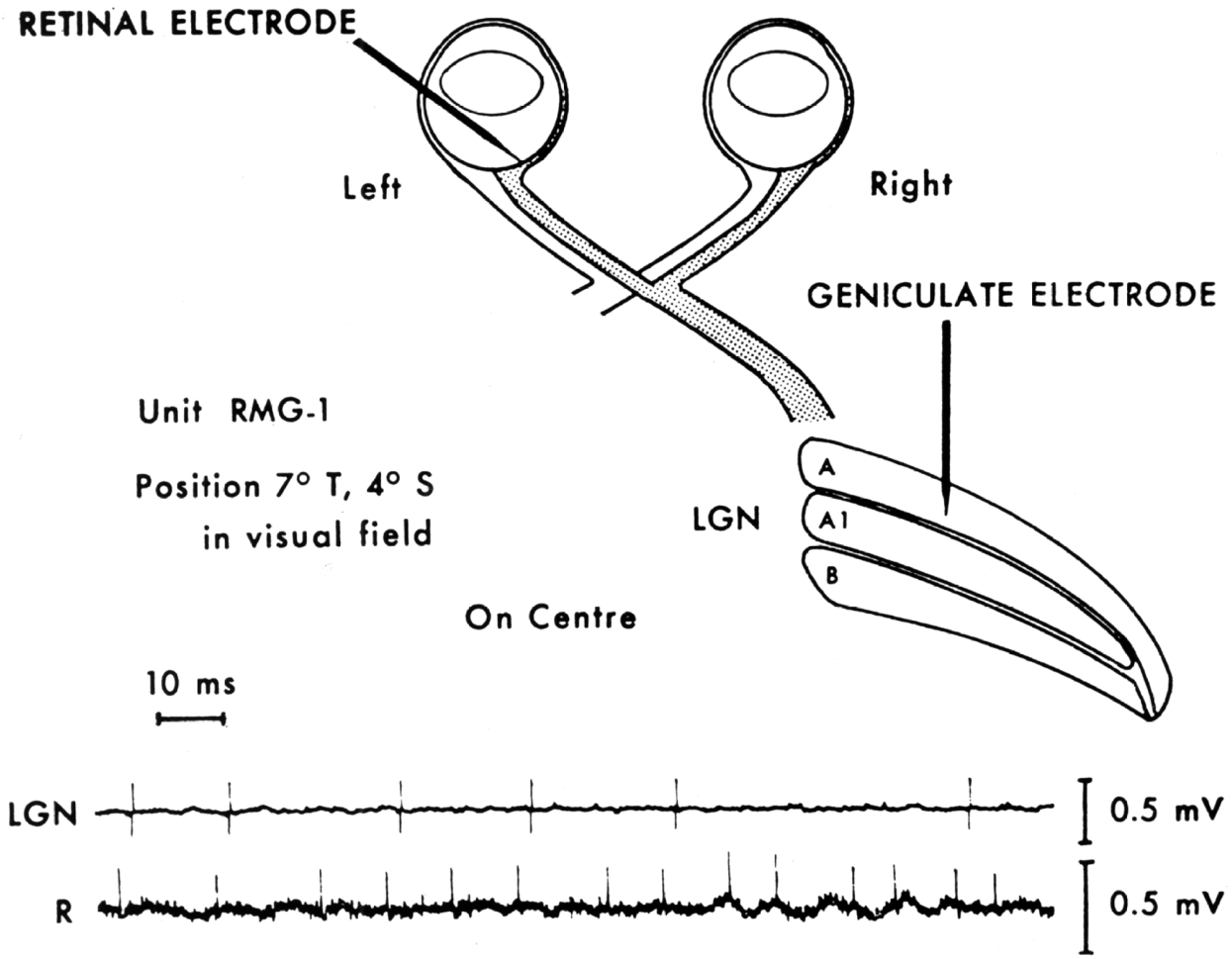

Cleland, Dubin & Levick (1971)

Responses in the retina and the LGN are more or less the same

Fig. 2 The receptive field plots at left are of an LGN neurone and two ganglion cells which directly excited it. (+) indicates response at "on", (−) indicates response at "off", (0) indicates no response. The size of the circles indicates the size of the test spot used, 0.7°. The receptive field outlines of the three units are also shown superimposed in their relative positions in the visual field, the LGN receptive field being stippled. The spike traces correspond to the LGN neurone and ganglion cell 1 as shown by connecting lines. The upper pair of traces show LGN spikes related, with a latency of about 2.5 ms, to spikes of ganglion cell 1. The arrows show two spikes that are not so related. In the lower set of traces, which are the superposition of a number of sweeps, both beams of the oscilloscope were triggered by the occurrence of a ganglion cell spike (lower beam). An S-potential (arrowed) is observed at the LGN neurone (upper beam), 2.5 ms after every retinal spike. Three S-potentials are seen to lead to spikes.

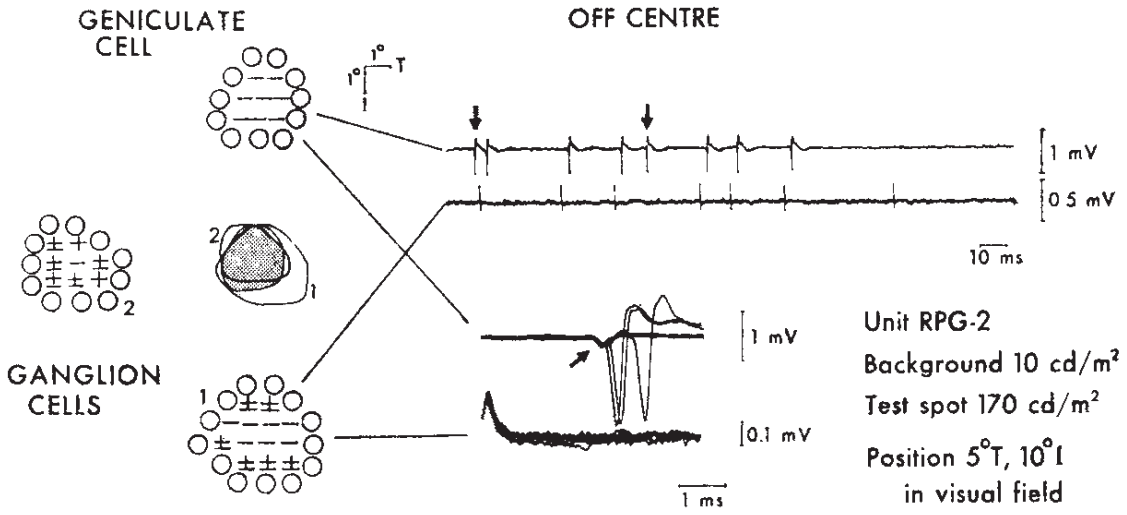

Cleland, Dubin & Levick (1971)

Basic properties of retinal EPSPs and LGN spikes.

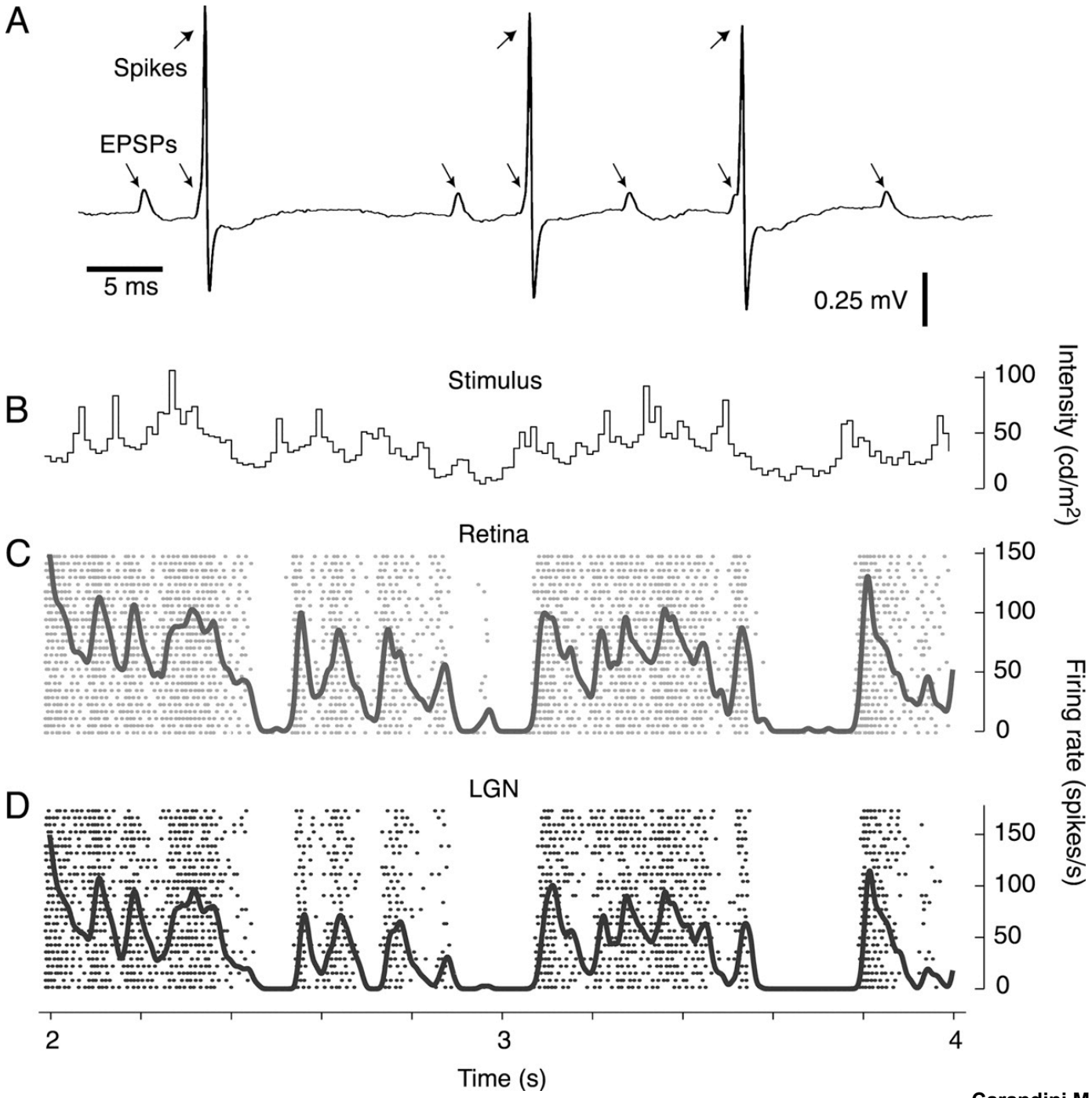

Journal of VISION
Carandini M et al. J Vis 2007;7:20

Efficacy of pairs of retinal spikes that occurred at different interspike intervals (ISIs)

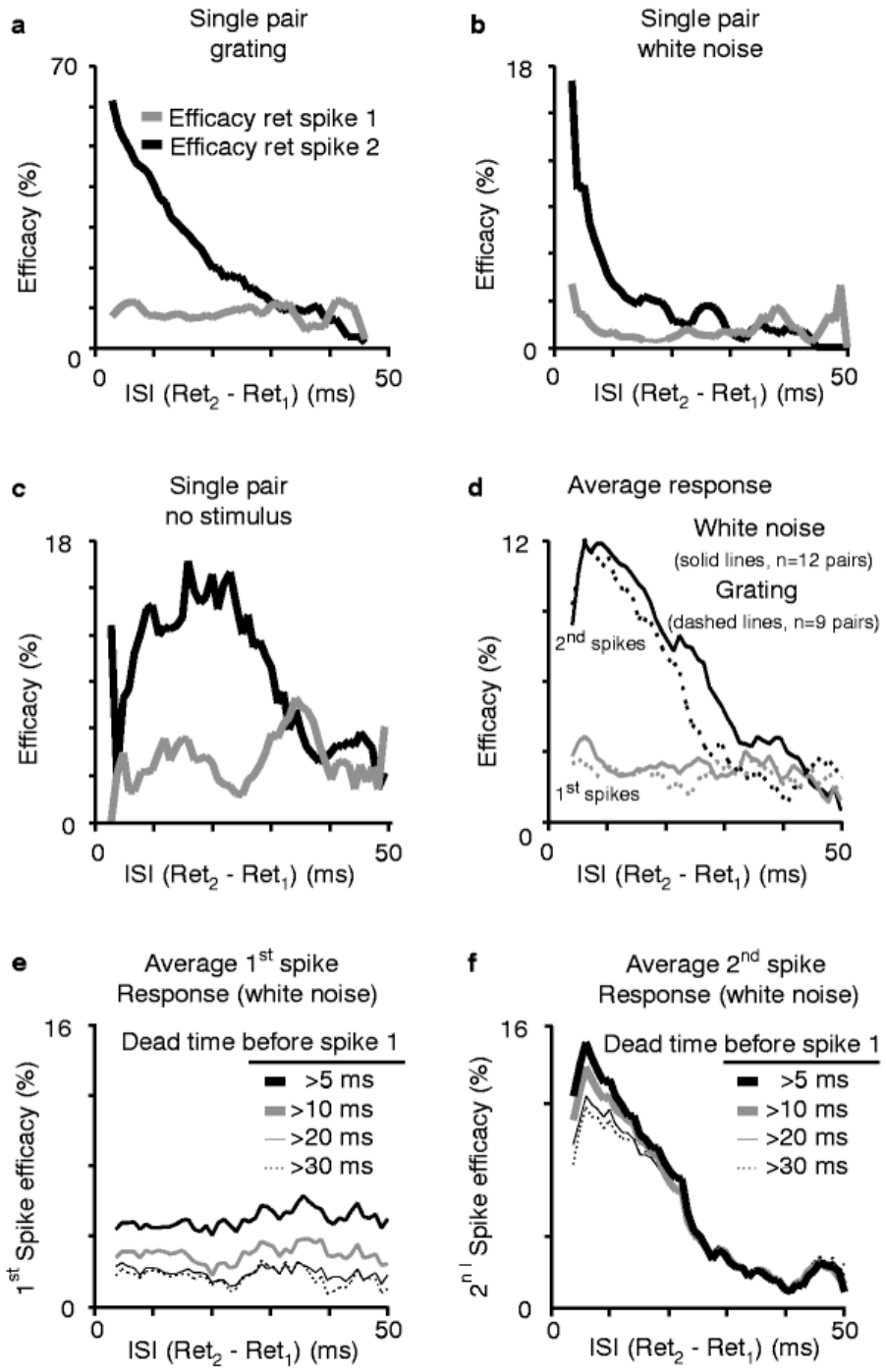

Usrey Reppas & Reid 1998

Predicting retinogeniculate integration with a summation model

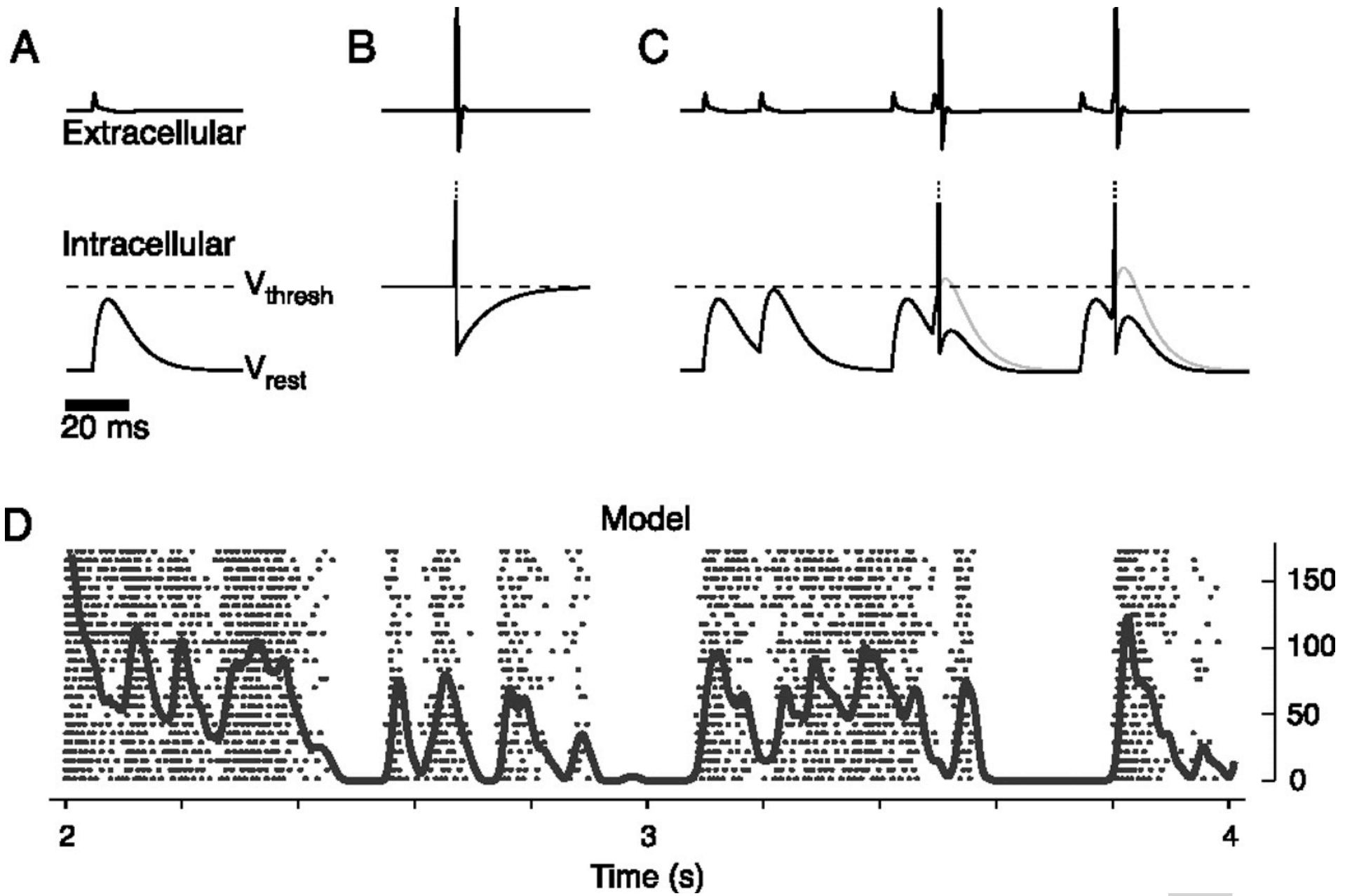

Journal of VISION
Carandini M et al. J Vis 2007;7:20

Comparison of observed and predicted synaptic efficacy

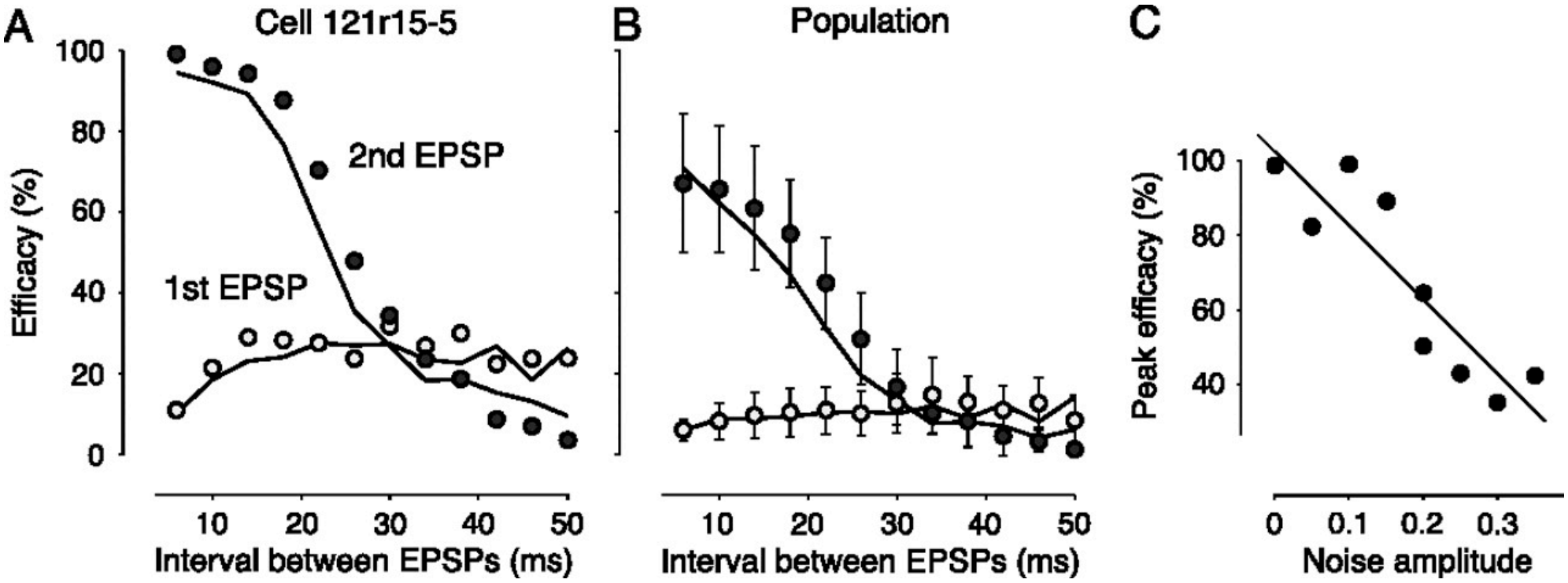

Carandini M et al. J Vis 2007;7:20

Comparison of contrast response functions from LGN neurons in alert and anaesthetized animals

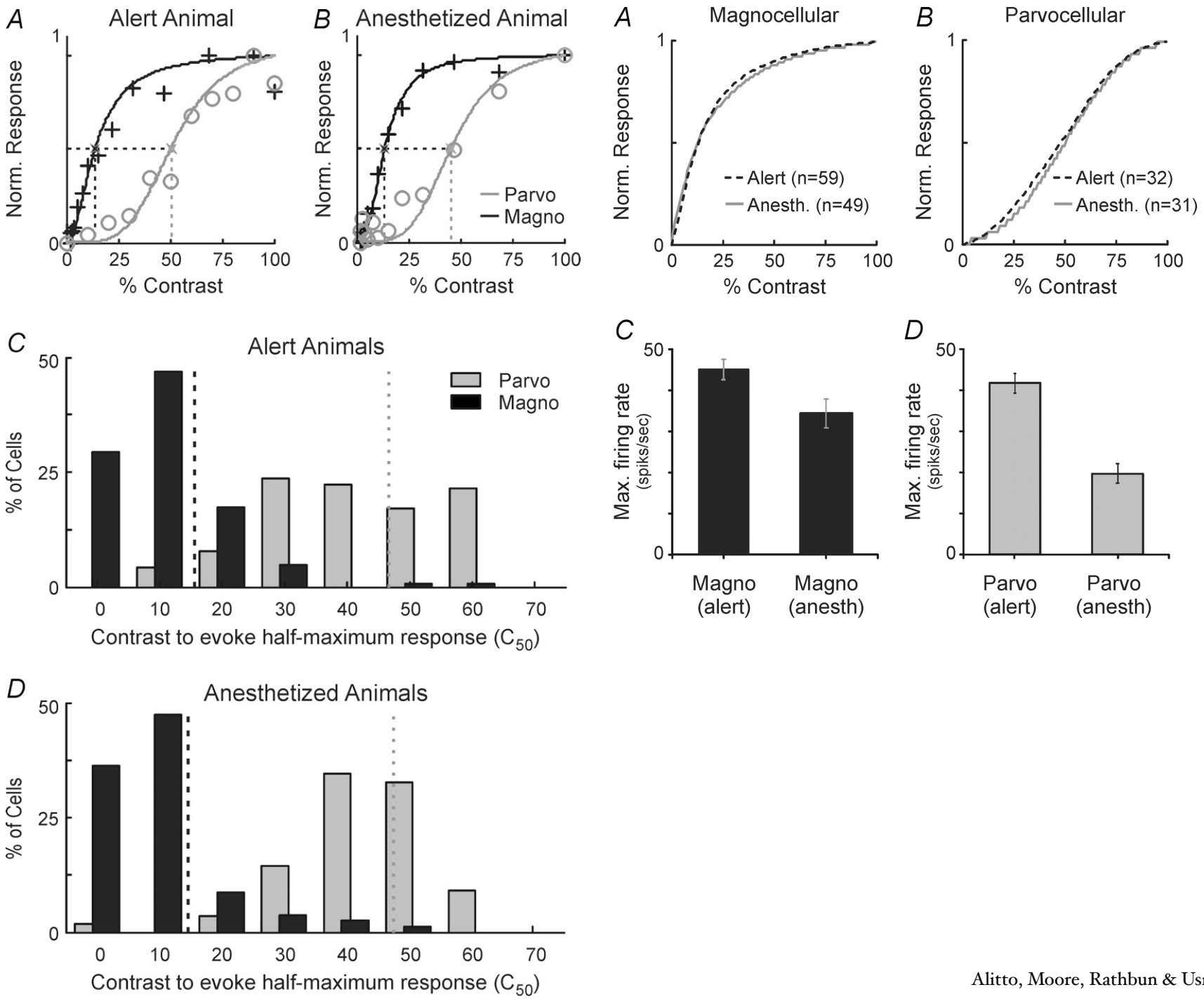

Alitto, Moore, Rathbun & Usrey (2011)

Comparison of temporal frequency tuning for LGN neurons in alert and anaesthetized animals

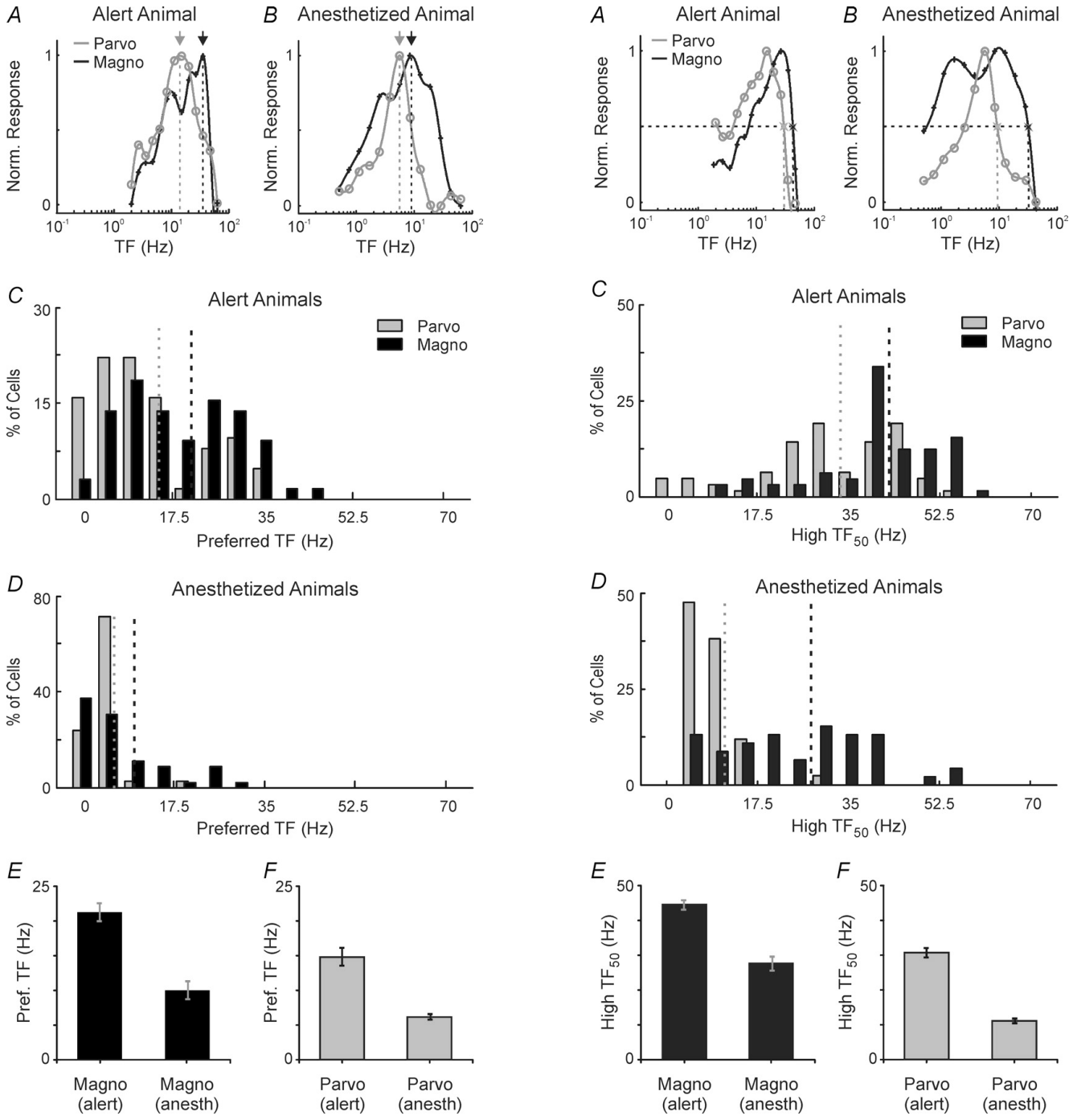

Alitto, Moore, Rathbun & Usrey (2011)